© 2022. Published by The Company of Biologists Ltd | Development (2022) 149, dev199573. doi:10.1242/dev.199573

RESEARCH ARTICLE

Uncoupling transcription and translation through miRNA-dependent poly(A) length control in haploid male germ cells

Mei Guo[1,*], Chunhai Luo[2,*], Zhuqing Wang[3,4,*], Sheng Chen[4,5], Dayton Morris[4], Fengying Ruan[1], Zhichao Chen[1], Linfeng Yang[1], Xiongyi Wei[2], Chuanwen Wu[1], Bei Luo[1], Zhou Lv[1], Jin Huang[1], Dong Zhang[1], Cong Yu[1], Qiang Gao[1], Hongqi Wang[1], Ying Zhang[2,‡], Fei Sun[2,‡], Wei Yan[3,4,6,‡] and Chong Tang[1,2,*,‡]

ABSTRACT

As one of the post-transcriptional regulatory mechanisms, uncoupling of transcription and translation plays an essential role in development and adulthood physiology. However, it remains elusive how thousands of mRNAs get translationally silenced while stability is maintained for hours or even days before translation. In addition to oocytes and neurons, developing spermatids display significant uncoupling of transcription and translation for delayed translation. Therefore, spermiogenesis represents an excellent *in vivo* model for investigating the mechanism underlying uncoupled transcription and translation. Through full-length poly(A) deep sequencing, we discovered dynamic changes in poly(A) length through deadenylation and re-polyadenylation. Deadenylation appeared to be mediated by microRNAs (miRNAs), and transcripts with shorter poly(A) tails tend to be sequestered into ribonucleoprotein (RNP) granules for translational repression and stabilization. In contrast, re-polyadenylation might allow for translocation of the translationally repressed transcripts from RNP granules to polysomes. Overall, our data suggest that miRNA-dependent poly(A) length control represents a previously unreported mechanism underlying uncoupled translation and transcription in haploid male mouse germ cells.

KEY WORDS: Poly(A) tail, MicroRNA, Deadenylation, Adenylation, RNP, Polysome, Spermiogenesis, Alternative splicing, Uncoupling of transcription and translation, Infertility, Mouse

INTRODUCTION

Once synthesized, transcripts undergo extensive post-transcriptional modifications in both the nucleus and cytoplasm (Keene, 2007). In the nucleus, precursor mRNAs are processed into mature mRNAs by removing introns through splicing and adding 5′ caps and 3′ polyadenylated [poly(A)] tails. The poly(A) tail is crucial for nuclear export, stability and translation of mRNAs (Goldstrohm and Wickens, 2008; Nicholson and Pasquinelli, 2019). In eukaryotic somatic cells, most poly(A) tails of cytoplasmic mRNAs are shortened over time through deadenylation (Elkon et al., 2013). The shortening of poly(A) tail leads to reduced translational efficiency and increased degradation. Interestingly, the poly(A) tails of mRNAs can also be lengthened through cytoplasmic polyadenylation in specific cell types, including oocytes, early embryos and neurons (Wormington, 1994; Richter, 1999; Ivshina et al., 2014). In mature oocytes, although mRNAs have shorter poly(A) tails (<20 nt), they are stable and stored in ribonucleoprotein (RNP) particles without being translated (Lim et al., 2016; Morgan et al., 2017). Soon after fertilization, these maternal transcripts are re-activated by cytoplasmic polyadenylation, which lengthens the poly(A) tails up to ∼80-150 nt, followed by efficient translation to produce proteins that are essential for survival and growth of the embryos, from fertilization to zygotic genome activation (two-cell embryo stage and four-cell embryo stage in mice and humans, respectively) (Gohin et al., 2014; Lim et al., 2016). The physiological significance of such a long delay in translation lies in the fact that postfertilization development before zygotic genome activation requires many proteins, which must be synthesized using pre-transcribed and stored maternal transcripts. In neurons, transcribed mRNAs tend to accumulate in the cell body, and these transcripts are sequestered into RNP granules, which travel a long distance and then start translation when reaching the axon terminals (Richter, 2001; Andreassi and Riccio, 2009; Norbury, 2013). Similarly, the translationally repressed mRNAs in neurons tend to have shorter poly(A) tails. Once they reach the synaptic junctions, these transcripts undergo cytoplasmic polyadenylation to lengthen their poly(A) tails, followed by an efficient translation (Curinha et al., 2014; Hilgers, 2015). These findings suggest that poly(A) length control represents an integral mechanism underlying uncoupled transcription and translation.

In addition to oocytes and neurons, haploid male germ cells (spermatids) also display uncoupled transcription and translation (Kashiwabara et al., 2008; Idler and Yan, 2012). As soon as round spermatids start to elongate, transcription is shut down owing to the onset of nuclear condensation. However, from the onset of spermatid elongation (step 9 in mice) to the completion of spermatid differentiation into spermatozoa (step 16 in mice), there are numerous steps through which structurally sound spermatozoa are assembled (Hermo et al., 2010; Idler and Yan, 2012). As transcription ceases upon elongation (step 9), all proteins needed for the remaining steps of sperm assembly (steps 9-16 in mice) have to

[1]R&D Department, BGI Genomics, BGI-Shenzhen, Shenzhen 518083, China. [2]Institute of Reproductive Medicine, Nantong University School of Medicine, Nantong University, Nantong 226001, Jiangsu, China. [3]Department of Physiology and Cell Biology, University of Nevada, Reno School of Medicine, 1664 North Virginia Street, MS575, Reno, NV 89557, USA. [4]Department of Endocrinology and Metabolism, The Lundquist Institute for Biomedical Innovation at Harbor-UCLA Medical Center, Torrance, CA 90502, USA. [5]China Medical University, Department of Laboratory Animal Science, Shenyang 110122, China. [6]Department of Medicine, David Geffen School of Medicine at UCLA, Los Angeles, CA 90095, USA.
*These authors contributed equally to this work

‡Authors for correspondence (tangchong@bgi.com; sunfei@ntu.edu.cn; wei.yan@lundquist.org; clairezhang@ntu.edu.cn)

Z.W., 0000-0002-3988-0733; S.C., 0000-0002-2089-3227; Y.Z., 0000-0002-7889-7124; F.S., 0000-0002-0870-8375; W.Y., 0000-0001-9569-9026; C.T., 0000-0002-6898-8946

Handling Editor: Haruhiko Koseki
Received 3 March 2021; Accepted 5 May 2022

Development (2022) 149, dev199573. doi:10.1242/dev.199573

be produced using transcripts synthesized before the transcriptional cessation, i.e., in round spermatids (steps 1-8) and even in late pachytene spermatocytes. For example, *Spata6* mRNAs start to be expressed in late pachytene spermatocytes, and its mRNA expression persists through the entire haploid phase. However, its protein is not detected until the sperm connecting piece/neck starts to assemble in step 9 spermatids (Yuan et al., 2015). Therefore, spermiogenesis, the process through which round spermatids differentiate into elongated spermatids and eventually spermatozoa, represents an excellent *in vivo* model for studying uncoupling of transcription and translation (Braun, 1998; Bettegowda and Wilkinson, 2010).

Uncoupling of transcription and translation in spermiogenesis is achieved through physical sequestration of mRNAs subjected to translational delay into the RNP granules, which exist as the nuage (also called intramitochondrial cement) in spermatocytes and the chromatoid body in round spermatids (Kotaja and Sassone-Corsi, 2007; Hermo et al., 2010). When spermiogenesis progresses to elongation steps, these mRNAs are gradually released from RNP granules and loaded onto polysomes to translate into the proteins required for sperm assembly (Braun, 1998; Bettegowda and Wilkinson, 2010; Hermo et al., 2010; Idler and Yan, 2012). Recent findings have shed light on the underlying molecular mechanisms. Briefly, our earlier work has revealed that RNP enrichment of mRNAs is a dynamic process, through which the overall length of 3′ untranslated regions (UTRs) becomes increasingly shortened compared with that of polysome-enriched mRNAs when late pachytene spermatocytes develop into the round and elongated spermatids (Zhang et al., 2017). The global 3′ UTR shortening is achieved through continuous shuffling of longer 3′ UTR mRNAs out of RNP granules followed by UPF1-3-mediated selective degradation (Bao et al., 2016) and by targeting shorter 3′ UTR mRNAs into RNP granules (Zhang et al., 2017). In this way, the overall 3′ UTR length of the entire mRNA transcriptome in elongating spermatids becomes shorter and shorter (Zhang et al., 2017). We have also reported data showing that both microRNAs (miRNAs) and m6A modification on pre-mRNAs are involved in the global shortening of transcripts and delayed translation (Tang et al., 2018, 2020). Precisely, proper m6A levels control correct splicing and, consequently, the expected length distribution of transcripts (Tang et al., 2018). Moreover, miRNAs target transcripts with longer 3′ UTRs through binding the distal binding sites to polysomes for translation followed by degradation, whereas transcripts with shorter 3′ UTRs only possess proximal miRNA binding sites, which, once bound by miRNAs, are targeted into RNP granules for stability and translational repression (Zhang et al., 2017).

Previous studies have shown that cytoplasmic poly(A) polymerases and poly(A) binding proteins are essential for spermiogenesis (Kleene et al., 1994; Kashiwabara et al., 2002, 2016; Yanagiya et al., 2010). However, it remains unknown how poly(A) length is regulated during global shortening of 3′ UTRs and dynamic translocation of mRNAs between RNP granules and polysomes during spermiogenesis, owing to technical difficulties in determining the full-length sequences of the poly(A) tails. Although both TAIL-seq and PAL-seq have been developed as the next generation sequencing (NGS)-based methods for determining poly(A) tail sequences (Chang et al., 2014; Subtelny et al., 2014), the short reads of NGS (<300 nt) do not allow for accurate determination of full-length poly(A) sequences, thus compromising the analyses on relationships among 3′ UTR length, poly(A) tail length, exon splicing patterns and translational status. To overcome this hurdle, we developed a sensitive method based on the third-generation PacBio sequencing, which we termed as poly(A)-PacBio sequencing (PAPA-seq), similar to FLAM-seq (Legnini et al., 2019). PAPA-seq can accurately measure poly(A) length with reads covering the entire 3′ ends and the full-length transcripts. Using this method, we determined the dynamic changes in poly(A) length in differentiating spermatids during spermatogenesis. Moreover, we found that miRNAs play an essential role in the regulation of poly(A) length and thus, delayed translation. For the first time, our data demonstrate a crucial role of miRNA-dependent poly(A) length control during spermiogenesis.

RESULTS

Dynamic changes in poly(A) length correlate with extended stability and delayed translation of mRNAs in developing haploid male germ cells

Given that the poly(A) tail is well-known to affect mRNA stability and translational efficiency (Goldstrohm and Wickens, 2008; Nicholson and Pasquinelli, 2019), we set out to measure the poly(A) length in spermatogenic cells using PAPA-seq (Fig. 1A,B), a sensitive method similar to FLAM-seq (Legnini et al., 2019). To construct libraries for PAPA-seq, the poly(U) polymerase was used to incorporate a limited number of G and I nucleotides to the 3′ end of poly(A)-selected RNA, and the reverse transcription was then performed to generate cDNAs containing the full-length poly(A) tails followed by sequencing using the PacBio system (Fig. 1B). Spike-in RNAs were sequenced to cross-validate the PAPA-seq data (Fig. S1). Using a modified STA-PUT method (Zhang et al., 2017), pachytene spermatocytes, round and elongating spermatids were purified from adult mouse testes with purities of 90%, 90% and 75%, respectively (Fig. 1A; Fig. S2).

Using PAPA-seq, we first examined the UTR length during spermatogenesis. Consistent with our previous report using short-reads sequencing (Zhang et al., 2017), PAPA-seq revealed that the 3′ UTRs of mRNAs were progressively shortened when pachytene spermatocytes developed into the round and elongating spermatids (Fig. S3A). A similar trend was also observed in the 5′ UTRs, but to a lesser extent (Fig. S3B). Supporting our previous finding that m6A-dependent splicing activities increase with the progression of spermiogenesis (Tang et al., 2018), further analyses of the PAPA-seq data also revealed increased splicing events (alternative exon, exon skipping etc.) when pachytene spermatocytes developed into the round and then elongating spermatids (Fig. S4A). The global shortening of 3′ UTRs might be related to enhancement of translational efficiency because shorter 3′ UTRs provide fewer binding sites for regulatory factors, including RNA-binding proteins and small non-coding RNAs (sncRNAs) (Jia et al., 2013; Bao et al., 2016; Zhang et al., 2017).

Although poly(A) length has long been known to influence mRNA stability and translational efficiency (Goldstrohm and Wickens, 2008; Nicholson and Pasquinelli, 2019), it remains unknown how the poly(A) length is regulated and whether the poly(A) length control is involved in uncoupling of transcription and translation during spermiogenesis. Despite the progressively shortened 3′ UTRs (Fig. S3) and decreased overall isoform transcript length (Fig. 1C), we found that the poly(A) tail length was dynamically regulated in a biphasic fashion from pachytene spermatocytes to round and elongating spermatids (Fig. 1D). The poly(A) tail length first increased from pachytene spermatocytes to round spermatids, which may contribute to the longer half-life of mRNAs that are pre-protected for delayed translation in late spermiogenesis (Phase I, Fig. 1D; Fig. S5). In contrast, from round to elongating spermatids, the poly(A) length gradually

Development (2022) 149, dev199573. doi:10.1242/dev.199573

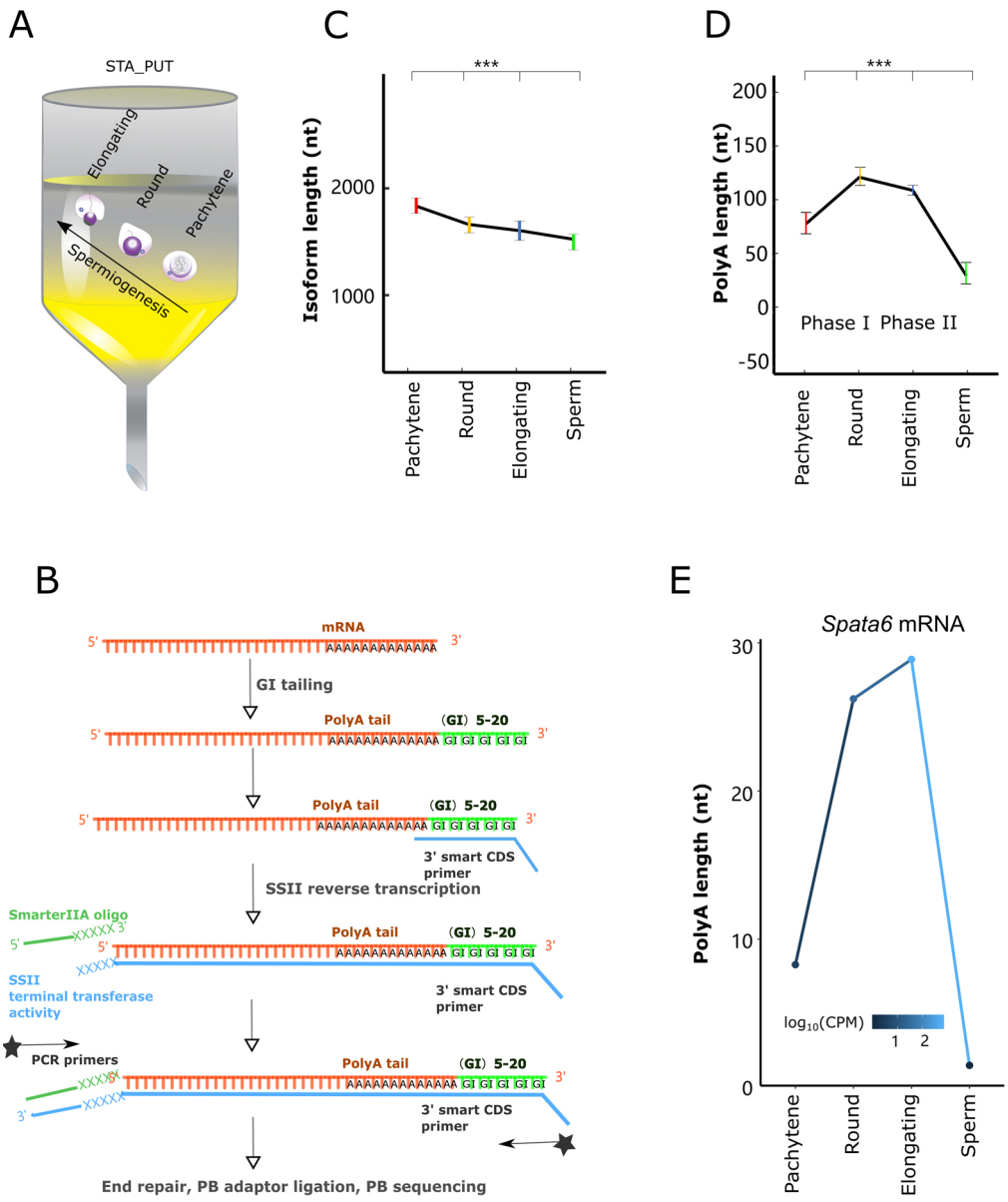

Fig. 1. Dynamic poly(A) length control during spermiogenesis as revealed by full-length poly(A) deep sequencing. (A) A gravity sedimentation-based STA-PUT method used to purify pachytene spermatocytes, round spermatids and elongating spermatids in the present study. (B) Schematic of PAPA-seq workflow. In brief, the poly(U) polymerase attaches poly(GI) tails to the very end of the poly(A) tail of RNAs. The modified poly(C) primer with adaptor sequence anneals to the poly(GI) tails. The reverse transcription, initiating from the start sites of poly(GI) tails, generates the cDNAs covering the full-length poly(A) tails. The other chemically modified adaptor is attached to the end of the cDNAs (i.e. corresponding to the 5′ ends of the RNA) by the template-switching activity of MMLV reverse transcriptase. PCR is then performed to amplify the cDNAs to a sufficient amount for PacBio library construction. Black star indicates PCR primers. (C) Average lengths of transcripts in pachytene spermatocytes, round and elongating spermatids, as well as spermatozoa. ***P<0.01, log unpaired one-tailed t-test, number of transcripts >20,000. Data were based on samples from two independent preparations with 3-6 mice in each, plus two technical replicates. (D) Line plot showing the average poly(A) length in pachytene spermatocytes, round and elongating spermatids, as well as spermatozoa. ***P<0.01, log t-test, number of transcripts >20,000. Data were based on samples from two independent preparations with 3-6 mice in each, plus two technical replicates. (E) Dynamic changes in the poly(A) length of *Spata6* transcripts during spermiogenesis. The x-axis represents for the male germ cell types, and the y-axis represents the mean poly(A) length. Counts per million reads mapped (CPM) is indicated by lines with blue gradients. *Spata6* mRNA levels increase from pachytene spermatocytes to round spermatids and then peak in elongating spermatids while the poly(A) tails are lengthening during the same period. Data were based on samples from two independent preparations with 3-6 mice in each, plus two technical replicates.

decreased (Phase II, Fig. 1D), suggesting that the shortening of the transcript poly(A) tails coincides with the delayed translation progressing. A good agreement was also found when comparing this result with those in the previous reports showing that shortening of the poly(A) tails correlates with translational activation in spermiogenesis (Kleene et al., 1984; Kleene, 1989). For example, transcript isoforms of *Spata6* mRNAs start to be expressed in late pachytene spermatocytes, and more isoforms continue to be expressed through the entire haploid phase. However, its protein is only expressed in the developing connecting piece in elongating (steps 9-12) and elongated (steps 13-16) spermatids (Yuan et al., 2015). We observed that the poly(A) length of *Spata6* drastically increased from pachytene spermatocytes to elongating spermatids, and this increase in poly(A) length occurred before the peak of

Development (2022) 149, dev199573. doi:10.1242/dev.199573

SPATA6 protein expression in elongated spermatids (Fig. 1E). Taken together, our PAPA-seq analyses revealed that mRNAs in round spermatids owned the longest poly(A) tails compared with pachytene spermatocytes and elongating/elongated spermatids despite the global shortening trend in overall length of the isoform transcripts. The increased poly(A) length synchronized with the delayed translation in spermiogenesis.

miRNAs mediate deadenylation of mRNAs enriched in RNPs

To further explore the effects of poly(A) length on mRNA translational repression and activation, we fractionated the cytosol of the three types of spermatogenic cells into RNP, mono- and polysome fractions using sucrose gradient centrifugation followed by PAPA-seq. By measuring OD_{254}, three fractions were observed: RNPs (the nuage/intramitochondrial cement in pachytene spermatocytes and the chromatoid body in round spermatids), monoribosome and polyribosome fractions (Fig. 2A). The purity of the fractions collected was validated through analyzing marker mRNAs well known for their distributions in RNP/polysome fractions (Fig. S6). Transcripts in the polysome fractions actively undergo translation, whereas those in the RNP fractions are translationally suppressed (Braun, 1998; Iguchi et al., 2006; Bettegowda and Wilkinson, 2010; Idler and Yan, 2012). Interestingly, through PAPA-seq, we found that the average poly(A) length of RNP-enriched mRNAs was only 1/40 of those enriched in the polysome fractions (Fig. 2B), suggesting a strong association between deadenylation of mRNAs and their localization to RNPs. This observation raises a crucial question: how are the mRNAs selected for deadenylation followed by sequestration in RNPs? Previous studies have shown that sncRNAs are enriched in RNPs (Zhang et al., 2017) and that argonaute proteins [e.g. AGO2, MIWI (PIWIL1) and MIWI2 (PIWIL4)] are abundant in the chromatoid body (Kotaja et al., 2006), suggesting a relationship between sncRNAs and deadenylation events of their target mRNAs. Following these clues, we hypothesized that the enhanced deadenylation of transcripts that are subjected to translational suppression in the RNP fractions during spermiogenesis might involve sncRNAs. To substantiate this hypothesis, we analyzed the miRNA-mRNA target relationship in RNPs and polysomes. We found that the miRNA targeting sites in the RNP-enriched transcripts appeared to be much more concentrated toward the 3′ ends compared with those in polysome-enriched transcripts in pachytene spermatocytes (Fig. 2C). When spermatogenesis progresses to round and elongating spermatid stages, the miRNA targeting sites at 3′ UTRs of the target transcripts gradually decreased and eventually disappeared, coinciding with the release of mRNAs from the chromatoid body/RNP in elongated spermatids (Fig. S7). The correlations among dynamic changes in miRNA targeting sites, mRNA sequestration and deadenylation suggest the involvement of miRNAs in these processes. This hypothesis is in agreement with previous reports, showing that miRNAs drive mRNAs into RNPs (Zhang et al., 2017) for deadenylation (Chen et al., 2009; Eulalio et al., 2009; Fabian et al., 2011; Eichhorn et al., 2016).

In somatic cells, miRNA-based deadenylation generally triggers the targeted mRNA decay (Chen et al., 2009). In contrast, the nuage and chromatoid body, which represent the RNP in spermatogenic cells functions to store transcripts (Peruquetti, 2015) and the fate of the deadenylated transcripts stored in RNP is not limited to decay. Further analyses of alternative polyadenylation site (APS) revealed that the vast majority of the RNP transcripts contain the APS motifs in the distal end of the 3′ UTRs, suggesting that these transcripts are not random degradation products (Fig. S8). To address the fate of deadenylated transcripts, we compared the poly(A) tail length distributions between RNP and polysome fractions in the three types of spermatogenic cells. Surprisingly, increased polyadenylation could be detected in both RNP and polysome fractions in round spermatids (Fig. S9). The presence of longer polyadenylated tails in polysome fractions could mean extended stability during translation, but how can we explain the longer polyadenylated transcripts in RNP fractions? These RNP-bound transcripts with longer poly(A) tails may function to move transcripts out of RNPs and reach the polysomes, thus switching from translational suppression to active translation. To test this hypothesis, we selected all of the transcripts with longer poly(A) tails in RNPs [>50 nt poly(A)] and examined their expression during spermiogenesis (Fig. 2D; Fig. S10). Indeed, levels of these transcripts decreased in RNP fractions but increased in polysome fractions from pachytene spermatocytes to round and elongating spermatids (Fig. 2D, framed by black dashed lines). In contrast, the transcripts with shorter poly(A) tails in RNPs (<5 bp) remained in the RNP fractions translationally repressed (Fig. 2E). A similar phenomenon was also observed in polyadenylated transcripts in round spermatid RNP fractions, in which the transcripts with longer poly(A) tails (>50 nt) moved out of the RNP fractions into polysome fractions, whereas those with shorter poly(A) tails (<5 nt) stayed in RNPs (Fig. S11). We also found that part of polyadenylated transcripts in RNPs quickly degraded in both RNP and polysome fractions (Fig. 2D, framed by blue dashed lines). These data may suggest that polyadenylated transcripts in the RNPs are either loaded onto the polysomes for active translation or subjected to degradation after translation (Fig. 2D; Fig. S11). However, it is difficult to provide the direct evidence to show the transcripts shifting between RNP and polysome. GO term enrichment analyses revealed that those polyadenylated transcripts encode proteins crucial for sperm assembly and sperm function, e.g., flagella development, acrosome assembly, motility and sperm-egg recognition, etc. (Fig. 2F). For example, *Spata6* is expressed as multiple isoforms during spermiogenesis and functions to assemble the sperm connecting piece/neck (Yuan et al., 2015). Once *Spata6* transcripts in the RNP phase gained the new long poly(A) tails [indicating the transcripts with re-polyadenylation or elongated poly(A) compared with the previous development stage) their levels dramatically decreased (Fig. 2G, left panel), whereas *Spata6* levels in polysome fractions were upregulated with a gradual increase in poly(A) tail length (Fig. 2G, right panel). Another classic example of delayed translation is protamine mRNAs (*Prm1* and *Prm2*) (Fig. S12). However, the poly(A) tails were cropped (50 bp) after releasing from RNP in the most abundant Prm isoform, suggesting that the suitable poly(A) length was required for delayed translation (Kleene, 1989). More interestingly, examination of the terminal sequences of all of the RNP-enriched transcripts revealed that the transcripts without new poly(A) tails (indicating the transcripts without polyadenylation compared with the previous development stage) displayed ∼10 times higher uridine content than the transcripts with new poly(A) tails [transcripts with re-polyadenylation or elongated poly(A) compared with the previous development stage] (Fig. S13D), suggesting a potential function of the uridine-rich motif in polyadenylation. Consistently, our ATAC-seq data (Tang et al., 2018) also show that most of the loci containing those re-polyadenylated mRNAs are already condensed in the pachytene and round spermatids (Fig. 2H; Fig. S14). Taken together, our data suggested that sncRNAs, especially miRNAs, likely mediate deadenylation of transcripts to be sequestered in RNPs, and the mRNAs with shorter poly(A) tails can be sequestered in RNPs.

Development (2022) 149, dev199573. doi:10.1242/dev.199573

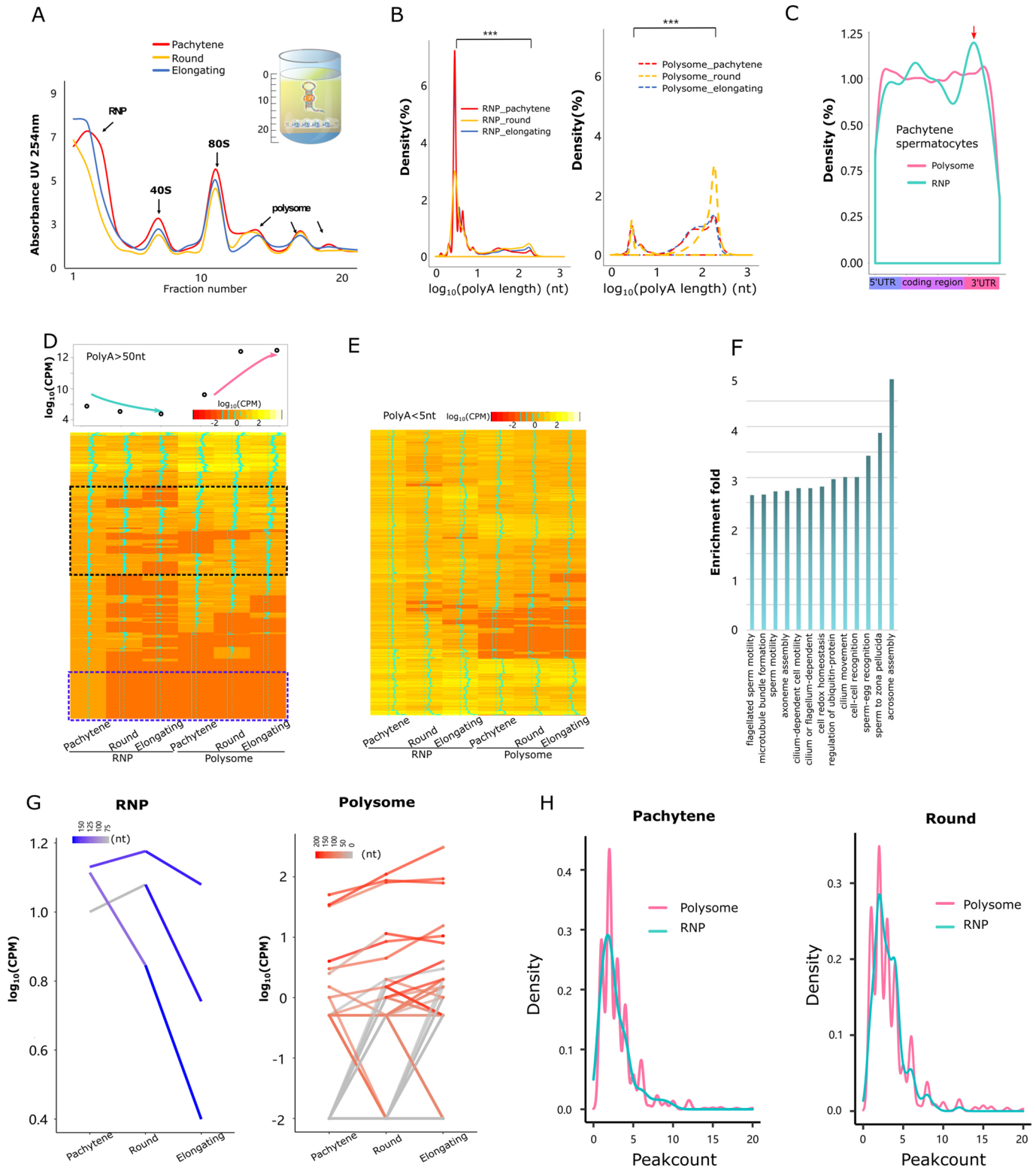

Fig. 2. See next page for legend.

miRNA ablation causes a failure in both poly(A) shortening and RNP phase separation in developing spermatids

To validate a role of miRNAs in poly(A) length control, we employed the *Drosha* conditional knockout (cKO) mouse model. *Drosha* encodes a nuclear RNase III enzyme essential for pre-miRNA cleavage (Han et al., 2006), and our previous study has shown that inactivation of *Drosha* exclusively in the spermatogenic cell linage through a cKO approach can abolish miRNA production in all developing male germ cells (Wu et al., 2012). Although *Drosha* cKO testes contain fewer spermatogenic cells due to germ cell depletion, there are still some pachytene spermatocytes, and round spermatids remained in the seminiferous epithelium

Development (2022) 149, dev199573. doi:10.1242/dev.199573

Fig. 2. Poly(A) length distribution in the RNP granules and polysome fractions. (A) The sucrose gradient centrifugation separates the RNP granules and polysome fractions from purified pachytene spermatocytes, round and elongating spermatids. The diagram shows the RNA abundance (*y*-axis) in RNP, monosome and polysome fractions (*x*-axis). (B) Density plots showing poly(A) length distribution in the RNP granules and polysomes in pachytene spermatocytes, round and elongating spermatids. The RNAs with shorter poly(A) tails are enriched in the RNP granules, with an average poly(A) length of 5 nt, whereas those with longer poly(A) tails are enriched in the polysome fractions, with an average length of 200 nt. ***P<0.01, log unpaired one-tailed *t*-test, number of transcripts >10,000. Data were based on samples from two independent preparations with 3-6 mice in each, plus two technical replicates. (C) Density plots showing distributions of the bioinformatically predicted miRNA targeting sites in transcripts enriched in RNP granules and polysome fractions in pachytene spermatocytes. The *y*-axis represents the density of the targeting sites and the *x*-axis shows the full-length mRNAs. The RNP-enriched miRNAs preferentially target the 3′ UTRs of mRNAs. (D) Heatmap showing that levels of mRNAs with the newly added longer poly(A) tails (>50 bp) gradually decrease in RNP granules and increase in the corresponding polysome fractions in the three spermatogenic cell types. The top panel shows the average expression levels of these mRNAs in each fraction. The *y*-axis shows mRNA expression level. The colors are scaled by the *z*-score. Green lines running in the center of heatmaps show the value of *z*-scores. (E) Heatmap showing that the levels of mRNAs with shorter poly(A) tails (<5 nt) do not significantly change in RNP fractions. Colored bar shows expression level of mRNA. (F) Gene Ontology (GO) term enrichment analyses of the mRNAs with longer poly(A) tails (>50 nt) in the RNP granules of three male germ cell types. The *y*-axis indicates enrichment fold. (G) Changes in expression levels of 26 *Spata6* isoforms in the RNP granules and polysomes. The *x*-axis indicates the three spermiogenic cell types, and the *y*-axis shows the levels/CPM of various isoforms. The specific color scheme corresponds to various poly(A) lengths. Levels of *Spata6* isoforms decrease with the increasing poly(A) length in RNP granules [darker blue indicates longer poly(A)]. In contrast, levels of *Spata6* isoforms increase with poly(A) lengthening [darker red indicates longer poly(A) in polysomes]. The log unpaired one-tailed *t*-test was used to determine the significance of the poly(A) change (P<0.1, between pachytene and elongating). Data were based on samples from two independent preparations with 3-6 mice in each, plus two technical replicates. (H) The signal counts indicated the ATAC signals in promoter regions in pachytene spermatocytes (left) and round spermatids (right). The pink line indicates the promoter regions, from which mRNAs are associated with polysomes and being actively translated. The cyan lines show the promoter regions, from which mRNAs are sequestered in RNP fractions. Generally, the transcriptionally active promoter regions have more than four signals. The promoters, from which mRNAs are sequestered in RNPs, appear to be less active than the polysome-associated promoters. CPM, counts per million reads mapped.

(Wu et al., 2012), which we purified and pooled for PAPA-seq analyses.

To test whether miRNAs deadenylate and sequester mRNAs into RNPs, we examined the effects of miRNA deficiency on the poly(A) length of their target mRNAs in *Drosha*-null spermatogenic cells. RNA contents in the RNP fractions of the *Drosha*-null pachytene spermatocytes and round spermatids were significantly lower than those in the wild-type controls (Figs 2A and 3A), suggesting that these transcripts might fail to accumulate in the RNP granules in the *Drosha* cKO male germ cells. Moreover, the ratio of gene numbers in RNP versus polysome fractions in *Drosha*-null spermatogenic cells reduced by >50% when compared with that in wild-type spermatogenic cells (Fig. 3B), further suggesting that in *Drosha*-null male germ cells, the transcripts failed to be compartmentalized to RNP granules in the absence of miRNAs. The fact that the mRNA levels in RNP fractions of *Drosha* cKO cells were drastically reduced compared with those in RNP fractions of wild-type cells (Fig. 3C) also supports this possibility, because the transcripts that failed to be localized to RNPs undergo massive degradation, leading to drastically reduced RNA levels. The results agree with the phenotype observed in the *Drosha* cKO mice (Wu et al., 2012), suggesting that ablation of miRNAs disturbs the delayed translation in spermiogenesis. Further analyses of the poly(A) length in different cell types and cytosolic fractions uncovered that the average poly(A) length of RNP-enriched transcripts in *Drosha*-null male germ cells was significantly longer than those in wild-type cells (Fig. 3D; Fig. S15), suggesting the relationship between miRNA and poly(A) reduction. The increased average poly(A) length in RNP-enriched transcripts in the *Drosha*-null germ cells most likely resulted from relative enrichment of longer poly(A) transcripts due to failed compartmentalization of the transcripts with trimmed poly(A) tails into the RNP granules in the absence of miRNAs. To further support this notion, we examined the dynamic poly(A) change between RNPs and polysomes in the wild-type and the *Drosha*-null round spermatids (Fig. 3E). We found that these *Drosha*-null transcripts failed to be sequestered into RNPs, and appeared to be stuck in the polysome fractions with very long poly(A) tails (Fig. 3E). It is also noteworthy that partial RNP-enriched transcripts in the wild-type round spermatids possessed much shorter poly(A) tails, and the same set of transcripts were mostly stuck in *Drosha*-null RNPs with much longer poly(A) tails (Fig. 3E, framed by black dashed lines). The miRNA influence on transcript deadenylation and translation status is possible. For example, in wild-type round spermatids, the multiple isoforms of *Spata6* were characterized by longer poly(A) in polysome and shorter poly(A) in RNP fractions (Fig. 3F). In sharp contrast, most of these transcripts were degraded in *Drosha* cKO cells, likely owing to mRNA degradation in the absence of miRNAs (Fig. 3F). As expected, a few transcripts with much longer poly(A) tails remained in the polysome fractions in *Drosha* cKO cells (Fig. 3F). Taken together, our data suggest that miRNA depletion might cause their targets to degrade and fail to compartmentalize RNAs into RNPs with poly(A) tail deduction.

X-linked miR-506 family miRNAs sequester *Fmr1* mRNAs into RNPs after deadenylation

While the overall changes in poly(A) length in *Drosha*-null male germ cells potentially support our hypothesis, it would be more convincing to demonstrate similar effects of depletion of specific miRNAs on the poly(A) length of their target mRNAs. Using the miR-506 knockout (KO) mouse line that we generated previously (Wang et al., 2020b), the effects of ablation of 18 miRNAs on their target mRNA, *Fmr1*, were investigated with an emphasis on poly(A) length and translational status. The miR-506 family contains 21 miRNAs transcribed from five large miRNA clusters encompassing a ∼62 kb region and a ∼22 kb region near *Slitrk2* and *Fmr1*, respectively, on the X chromosome, most of which are preferentially expressed in the testis (Wang et al., 2020b). The KO line used in this study lacks 18 out of 21 miRNAs of the miR-506 family (Wang et al., 2020b). *Fmr1* has been validated using both western blots and luciferase assays (Ramaiah et al., 2019; Wang et al., 2020b) (Fig. 4A). *Fmr1* and the miRNA-506 family were both expressed in RNP/polysome fractions of spermatogenic cells (Fig. S16). We first analyzed *Fmr1* mRNA levels using a semi-quantitative PCR and found no changes in *Fmr1* levels in KO testes (Fig. 4B; Fig. S17), indicating that miR-506 did not degrade its target *Fmr1*. As shown in our previous report (Wang et al., 2020b), FMRP levels were reduced by ∼50% in the miR-506 family KO testes compared with the wild-type controls (Fig. 4B, middle panel). To unveil the differential patterns between mRNA and protein, we further examined the poly(A) length in the miR-506 family KO and

Development (2022) 149, dev199573. doi:10.1242/dev.199573

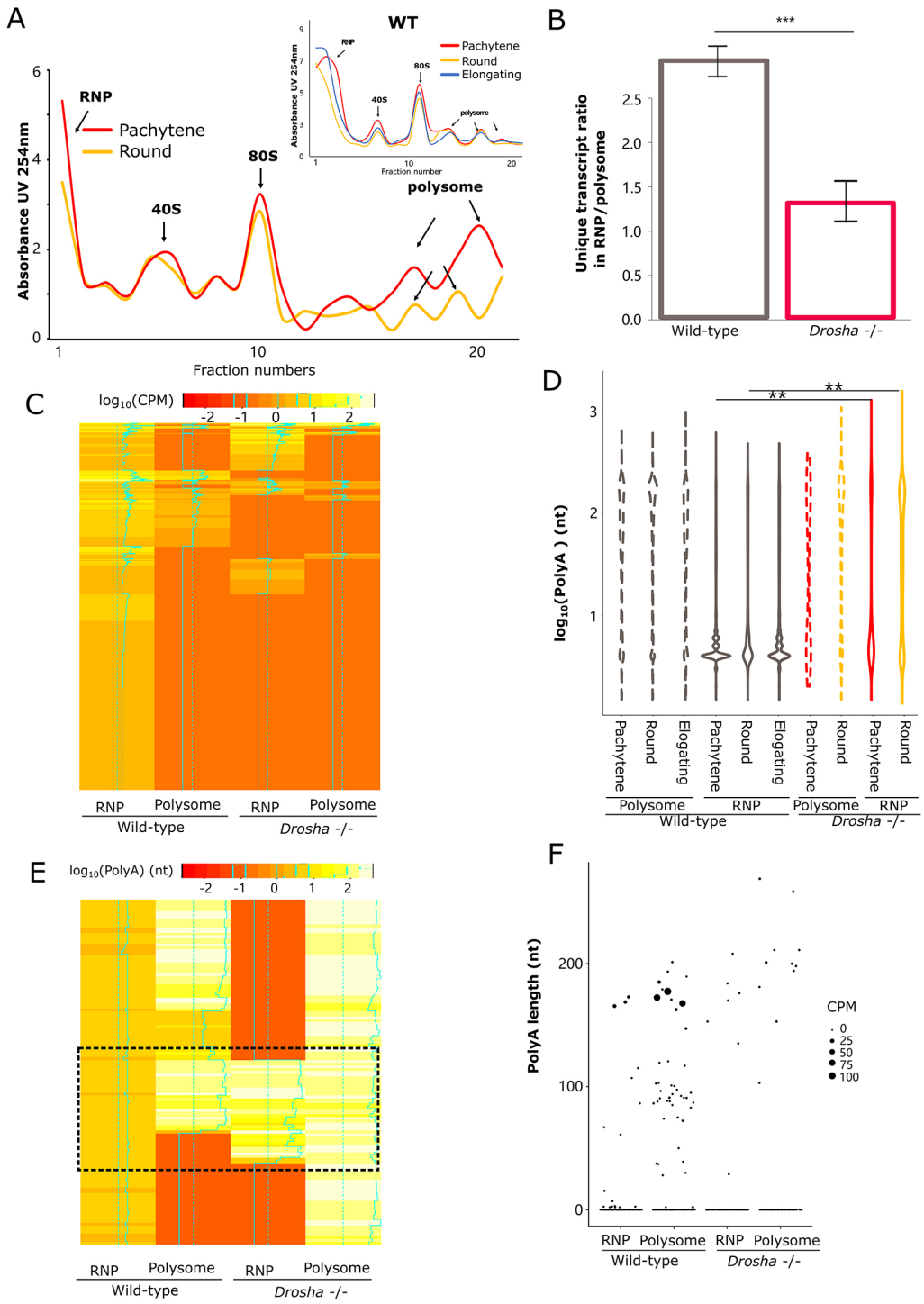

Fig. 3. See next page for legend.

wild-type testes using a poly(A) length PCR assay, as described previously (Kusov et al., 2001). Interestingly, the average poly(A) length of the *Fmr1* mRNAs appeared to be doubled in the miR-506 KO testes (Fig. 4D, left panel), suggesting that the poly(A) length indeed affects protein translation efficiency. The poly(A) pattern of the miR-506 family KO mice was consistent with that of the *Drosha* cKO mice, supporting the suggestion that miRNAs in the testis may function to trim poly(A) tails to achieve RNP compartmentalization and delayed translation. Based on our proposed model, the *Fmr1* mRNA would not be able to be deadenylated and sequestered into RNP granules in the absence of miR-506 family miRNAs. Indeed, our data showed that *Fmr1* mRNAs levels decreased by ∼10% in RNP granules (Fig. 4C). Moreover, the poly(A) tails of *Fmr1* mRNAs in RNPs are much longer in the miR-506 family KO testes than those in the wild-type testes (Fig. 4D, right panel), and no significant difference were observed in the polysome fractions (Fig. 4D). These findings are generally consistent with other genes (e.g. *Skp2* and *Snai2*) found in the miR-506 KO testes (Fig. 4D). Overall, these results further support our hypothesis that miRNAs shorten the poly(A) length of their target mRNAs through

Development (2022) 149, dev199573. doi:10.1242/dev.199573

Fig. 3. Effects of miRNA deficiency on the poly(A) length distribution in the RNP granules and polysome fractions. (A) Distribution of RNA contents in the RNP and polysome fractions in purified *Drosha*-null pachytene spermatocytes and round spermatids and wild type (upper left). (B) Bar graphs showing the ratio of RNP-enriched versus polysome-enriched transcripts in wild-type and *Drosha*-null pachytene spermatocytes and round spermatids. ***P<0.01, Wilcoxon rank test. Wild-type samples were from two independent preparations with 3-6 mice in each, plus two technical replicates. *Drosha* KO samples were from single preparation with 6-10 KO testes plus two technical replicates. Data are mean±s.d. (C) Heatmap showing the expression levels of RNP-enriched transcripts in wild-type round spermatids are generally downregulated in both RNP and polysome fractions in *Drosha*-null round spermatids. The colored bar indicates mRNA expression level. The colors are scaled by the *z*-score. Green lines running in the center of heatmaps show the value of *z*-scores. (D) Violin plots showing the poly(A) length distribution in the RNP and polysome fractions of wild-type and *Drosha*-null spermatogenic cells. **P<0.05, unpaired one-tailed Student's *t*-test, number of transcripts >10,000. Wild-type samples were from two independent preparations with 3-6 mice in each, plus two technical replicates. *Drosha* KO samples were from a single preparation with 6-10 KO testes plus two technical replicates. (E) Heatmap showing poly(A) length of transcripts enriched in RNP in wild-type round spermatids are largely absent in the RNPs of *Drosha*-null round spermatids, and these appear to be stuck in the polysome fractions with elongated long poly(A) tails. Partial transcripts also could bind to RNPs with long poly(A) tails (black dashed square). The colored bar indicates mRNA poly(A) length. The colors are scaled by the *z*-score. Green lines running in the center of heatmaps show the value of Z-scores. (F) Dot plot showing the distribution of the abundance of *Spata6* isoforms with different poly(A) length in both RNP and polysome fractions of wild-type and *Drosha*-null round spermatids. Log *t*-test was used to determine the RNA enrichment in RNP or polysome, P<0.05. Wild-type samples were from two independent preparations with 3-6 mice in each, plus two technical replicates. *Drosha* KO samples were from a single preparation with 6-10 KO testes plus two technical replicates.

deadenylation to sequester them in RNP granules for delayed translation.

DISCUSSION

Uncoupling of transcription and translation is prominent during spermiogenesis (round spermatid differentiation into spermatozoa) (Braun, 1998; Bettegowda and Wilkinson, 2010; Idler and Yan, 2012), oogenesis (maternal transcript production) (Bettegowda and Smith, 2007; Sha et al., 2019), preimplantation embryonic development (protein production before zygotic genome activation) (Cui and Kim, 2007; Gohin et al., 2014; Lim et al., 2016) and neuronal cell functions (mRNA synthesis in the cell body and translation in the axon) (Richter, 2001; Andreassi and Riccio, 2009; Norbury, 2013). Several potential mechanisms have been identified to achieve uncoupled transcription and translation, including physical sequestration of mRNAs and proteins in RNP granules (Braun, 1998; Bettegowda and Wilkinson, 2010; Zhang et al., 2017), 3′ UTR length control through alternative polyadenylation (Di Giammartino et al., 2011; Mayr, 2017) and 3′ UTR length-dependent selective decay of transcripts by UPF proteins (Boehm et al., 2014; Bao et al., 2016). The poly(A) length has long been known to regulate transcript stability and translational efficiency (Goldstrohm and Wickens, 2008; Nicholson and Pasquinelli, 2019). However, investigations into the role of poly(A) length control have just begun to emerge (Morgan et al., 2017; Legnini et al., 2019; Liu et al., 2019; Nicholson and Pasquinelli, 2019). This is primarily due to a lack of sensitive methodologies that allow for accurate determination of the full-length poly(A) tail sequences. The third-generation deep sequencing technologies, e.g., PacBio and Nanopore sequencing, allowed us to develop a sensitive method, which we termed PAPA-seq, to determine the full-length sequences of not only poly(A) tails but also the rest of the entire transcripts. There are several design differences between FLAM-seq (Legnini et al., 2019) and PAPA-seq, although the overall concept is similar. First, FLAM-seq was tailed by G and I bases using the USB poly(A) length assay kit (764551KT, Thermo Fisher Scientific), which is proprietary. In our protocol, we demonstrated that the GI tail could be effectively added by poly(U) polymerase (M0337, New England Biolabs) in the precise GI mixing concentration. Second, we tested many different oligos and identified the one with the highest efficacy in batch testing. These oligos could generate fewer dimers in the PCR. Lastly, the oligo modification is different. Specifically, FLAM-seq used iCiGiCAAGCAGTGGTATCAACGCAGAGTA-CATrGrGrG. We used the LNA modification in the 3′ end to increase the template switching activity. Using PAPA-seq, we discovered that the average length of the poly(A) tails is ∼100 nt. However, it can be as long as 1000 nt in some transcripts in the three spermatogenic cell types (pachytene spermatocytes, and the round and elongating spermatids). The poly(A) tails are much longer in round and elongating spermatids than those in pachytene spermatocytes. This pattern aligns well with the highest number of transcripts subjected to delayed translation in round and elongating spermatids, compared with pachytene spermatocytes. As longer poly(A) tails tend to have enhanced stability and translational efficiency, the peak of poly(A) lengthening in round and elongating spermatids may reflect the peak of delayed translation of those pre-synthesized, RNP-enriched transcripts.

Previous reports have shown that poly(A) binding proteins (PABPs) interact with the deadenylation complex (CCR4-NOT-Tob and PAN2-PAN3) to cause increased mRNA decay and repressed translation by shortening their poly(A) tails (Flamand et al., 2016; Yi et al., 2018). However, this mechanism targets all transcripts, causing massive degradation, whereas in developing spermatids with uncoupled transcription and translation, deadenylation occurs in the transcripts to be sequestered into the RNP granules. The selective deadenylation must be mediated by a factor with sequence specificity, e.g., miRNAs. Indeed, our data strongly support such a role of miRNAs. Therefore, miRNAs appear to play an important role by regulating the poly(A) length through binding their target mRNAs. In spermatogenic cells, miRNAs count for ∼10% of total sncRNAs (Zhang et al., 2017). Other sncRNAs, for example, tsRNA and piRNA, may also be able to sequester mRNAs into RNPs (Vourekas et al., 2012; Kim, 2019). Moreover, the molar ratio of sncRNAs versus large RNAs in RNPs is over 100:1, implying that the excessive amount of sncRNAs may target other regions of mRNAs to translocate mRNAs (Zhang et al., 2017). Therefore, in the absence of miRNAs, the mRNAs with pure poly(A) tails cannot be deadenylated and thus, failed to be compartmentalized into the RNP granules. However, a few transcripts remain associated with RNPs, which may be due to other targeting sncRNAs and/or poly(A) patterns. It is noteworthy that cytosine-enriched poly(A) tails still can manage to be phase-separated into RNP granules because the cytosine-enriched poly(A) tails have much reduced PABP binding affinity when compared with the pure poly(A) tails (Lunde et al., 2007) and are therefore more capable of changing their internal structures to increase hydrophobicity, driving RNP phase separation independent of miRNA-mediated deadenylation. Even if the miRNA depletion caused the massive RNA degradation, some RNAs (*Spata6*) could preserve the longer poly(A) to maintain the longer stability in order to support the essential protein expression. Overall, the miRNA binding is crucial, but not the only factor to sequester the transcripts into RNPs. Other factors, such as RNA binding proteins, non-A nucleotide distribution in poly(A) tails and other sncRNAs could also affect the mRNA storage in RNPs.

Development (2022) 149, dev199573. doi:10.1242/dev.199573

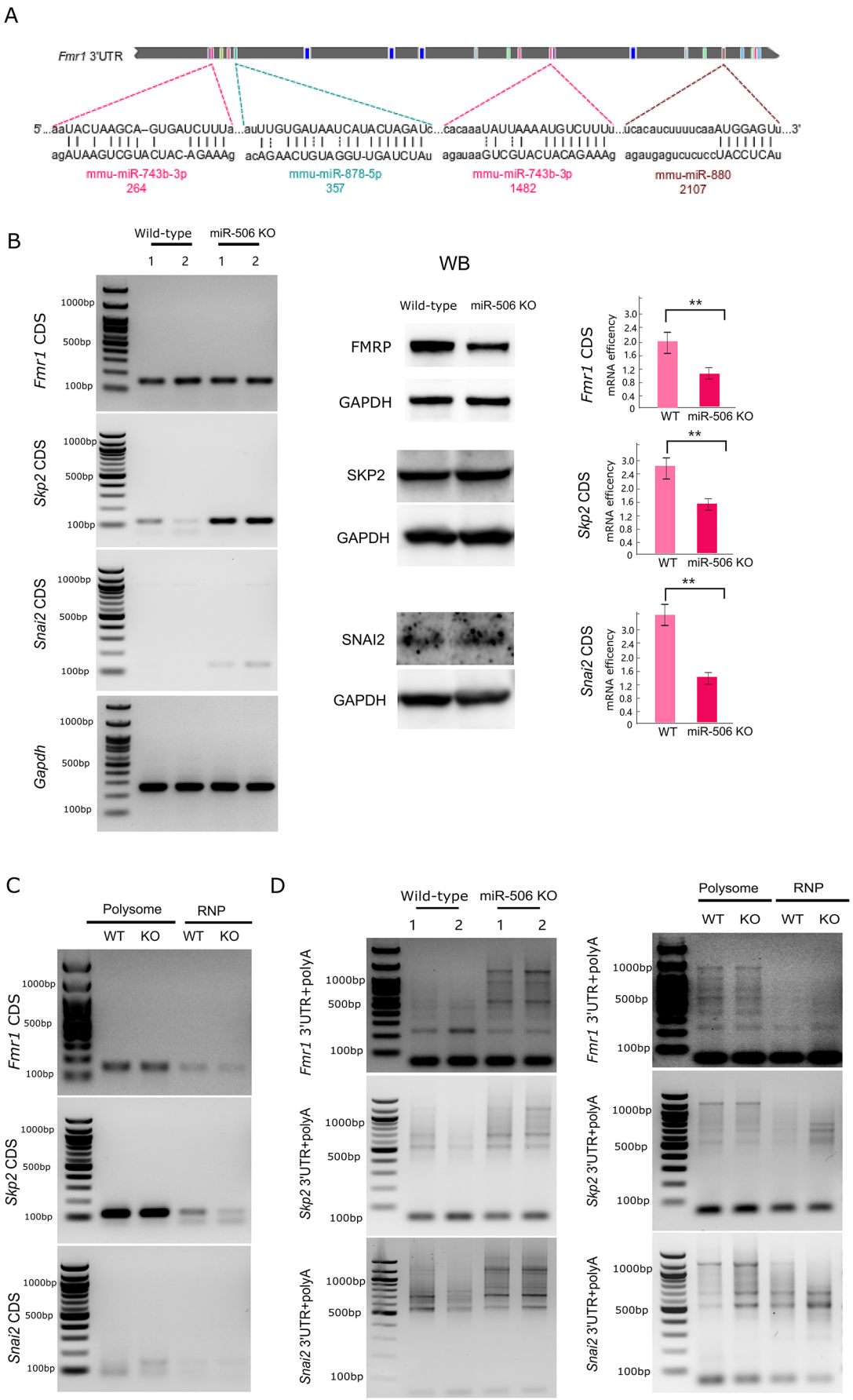

Fig. 4. See next page for legend.

Development (2022) 149, dev199573. doi:10.1242/dev.199573

Fig. 4. miR-506 family miRNAs regulate the poly(A) length of their target gene *Fmr1* in the testis. (A) Schematic showing the targeting sites in *Fmr1* 3′ UTR by four of the miR-506 family, as previously reported (Ramaiah et al., 2019). (B) Left: semi-quantitative RT-PCR analyses on levels of *Fmr1*, *Skp2* and *Snai2* mRNA (CDS for coding sequences) in total testes of the miR-506 family KO and wild-type male mice. *Gapdh* was used as the loading control. Middle: western blot analyses of Fmr1 protein (FMRP), SKP2 and SNAI2 levels in the miR-506 family KO and wild-type testes. GAPDH was used as the loading control. Right: histograms show mRNA translation efficiency (protein expression/mRNA expression), displaying quantitative analyses of the data (mean±s.e.m.) from biological triplicates (n=3). $^{**}P$<0.05 (unpaired one-tailed Student's t-test). (C) Semi-quantitative RT-PCR analyses on levels of *Fmr1*, *Skp2* and *Snai2* mRNA (CDS for coding sequences) in fractions of RNP and polysome of the miR-506 family KO and wild-type male mice. (D) Distribution of the poly(A) length of *Fmr1*, *Skp2* and *Snia2* mRNAs in total testes of the miR-506 family KO and wild-type control male mice. The panels are representative gel images, indicating the poly(A) tail-lengths of *Fmr1*, *Skp2* and *Snai2*, which are the sizes of poly(A) PCR-amplified products plus the length of the gene-specific forward primer to the putative polyadenylation start site. Numbers 1 and 2 indicated the two replicates of the whole testes. KO and WT denote the miR-506 family KO and wild-type testes, respectively. Elongation of miR-506 target poly(A) in the miR-506 KO, compared with wild-type controls, and the poly(A) elongation appears to occur in the RNP rather than polysome fractions.

The lack of germ cell depletion in miR-506 KO testes makes this KO mouse line advantageous due to minimal secondary effects. *Fmr1* protein FMRP levels decrease by half, whereas its mRNA levels remain unchanged despite their poly(A) tails doubling their length in the absence of 18 *Fmr1*-targeting miRNAs in the KO testes *in vivo*. This finding is surprising because it is against the common belief that miRNAs degrade the target mRNAs in somatic cells (Shyu et al., 2008). However, this result does support our proposed model in spermiogenesis. Specifically, in the absence of targeting miRNAs, the mRNAs fail to be deadenylated. Although *Fmr1* mRNAs managed to get into RNPs, their translation in elongating and elongated spermatids does not occur normally, leading to a decreased protein level, because of the dysregulated poly(A) tails. This is in sharp contrast to the wild-type situation where *Fmr1* with shorter poly(A) tails are stored in RNPs, supporting our notion that miRNAs trigger the deadenylation of their targeted mRNAs, and deadenylation of mRNAs effectively controls the delayed protein translation in spermiogenesis.

The function of the chromatoid body is still a source of debate, but the general consensus is that the chromatoid body determines the transcript fate: degradation or storage for delayed translation (Matsui et al., 2000; Keeling et al., 2006; Kotaja and Sassone-Corsi, 2007; Moser and Fritzler, 2010, 2013; Meikar et al., 2011; Ostareck-Lederer and Ostareck, 2012; Piccolo et al., 2014; Hofweber and Dormann, 2019). Disturbing the chromatid body components caused severe defects in spermiogenesis (Vasileva et al., 2009). However, a definitive link between poly(A) length and the dynamic changes of transcripts between RNP and polysome subcytoplasmic compartments has been challenging to prove. Here, we report a clear association between the poly(A) length and translational status, as reflected by relative enrichment in the RNP and polysome fractions. Our inference is that the RNP-stored transcripts are re-adenylated and shifted to polysomes for delayed translation in later developmental stages, which represents a model for the delayed translation in spermiogenesis. However, the present study is limited by difficulties in distinguishing the early stored transcripts from the nascent RNAs in the re-polyadenylated RNA population, considering transcription remains active in round spermatids. Therefore, it is also possible that the transcripts in RNPs were degraded directly without re-adenylation, and the same mRNAs on the polysomes represent nascent mRNAs. However, the fact that the re-polyadenylated mRNAs in round spermatids display a similar shift from RNP to polysomes in the elongating spermatids, in which transcription has long ceased, suggest that re-polyadenylation occurs to the pre-existing rather than nascent mRNAs. Nevertheless, further experimental evidence showing depolyadenylation and re-polyadenylation on the same transcript is warranted. Of course, the possibility that the polyadenylated mRNAs in RNPs are mainly nascent mRNAs does exist. In summary, here, we have reported evidence supporting miRNA-dependent poly(A) length control in male germ cells, which represents a mechanism underlying uncoupled transcription and translation in the haploid phase of spermatogenesis.

MATERIALS AND METHODS

Animals

All wild-type and KO mice used in this study were on the C57BL/6J background and housed under specific pathogen-free conditions in a temperature- and humidity-controlled animal facility at the Nantong University (China) and the University of Nevada, Reno (USA). The animal protocols were approved by the Animal Care and Use Committee of Nantong University or University of Nevada, Reno. Male germ cell-specific *Drosha* conditional KO mice ($Drosha^{loxp/loxp}$ mice were bred with *Stra8-iCre* mice) and global KO of X-linked miR-506 family were generated and genotyped at the University of Nevada, Reno as previously described (Wu et al., 2012; Zhang et al., 2017; Wang et al., 2020a,b) (Fig. S18).

Mouse genotyping

Mouse tail or ear snips were lysed in 120 µl of lysis buffer (40 mM NaOH, 0.2 mM EDTA, pH 12) for 30 min∼1 h at 95°C, followed by neutralization with 120 µl of neutralizing buffer containing 40 mM Tris-HCl (pH 5) as previously described (Wang et al., 2020a). PCR reactions were conducted using the GoTaq Green master mix (M7123, Promega). The PCR conditions were as follows: initial denaturation at 95°C for 2 min, followed by 35 cycles of amplification (denaturation at 95°C for 30 s, annealing at 55°C for 30 s, and elongation 72°C for 1 min) with a final elongation at 72°C for 5 min. The primers used for genotyping are listed in Table S1.

Purification of spermatogenic cells

Pachytene spermatocytes, round and elongating/elongated spermatids were purified from adult mouse testes using the STA-PUT method (Zhang et al., 2017). The bovine serum albumin (BSA) gradients (0.5-4%) were prepared in the EKRB buffer (K-4002, Sigma-Aldrich), supplemented with sodium bicarbonate (1.26 g/l), L-glutamine (0.29228 g/l), Penicillin and Streptomycin mix (Thermo Fisher Scientific, 10,000 U/l), MEM non-essential amino acids (Thermo Fisher Scientific, 1 ml 100× per l), MEM amino acids (20 ml 50× per l) and cycloheximide (100 ng/ml) (pH 7.2-7.3). Eight testes were pooled each time for cell purification. After being collected and decapsulated, testes were placed into 10 ml of the EKRB buffer containing 5 mg collagenase (Sigma-Aldrich) for 12-min digestion at 32°C to disperse the testicular cells. Once dispersed, the testicular cells were washed three times using the EKRB buffer followed by trypsin digestion by incubation in 10 ml EKR buffer containing trypsin (Sigma-Aldrich, 0.25 mg/ml) and DNase I (Sigma-Aldrich, 20 µg/ml) at 37°C for 12 min with occasional pipetting to facilitate cell dispersion. Thoroughly dispersed testicular cells were washed three times, followed by centrifugation (at 800 ***g*** for 10 min) and re-suspension in 10 ml of 0.5% BSA. The cell suspension was passed through 50 µm filters and the filtrate was saved for loading onto the STA-PUT apparatus for sedimentation. After 3 h sedimentation at 4°C, fractions were collected from the bottom of the sedimentation chamber. A total of 30 fractions of 15 ml each were collected. After centrifugation, the supernatants were removed and the cells in each fraction were re-suspended. The cell purity was determined by microscopy examination based on cell morphology, as described previously (Morgan et al., 2019). Fractions containing the same cell types were pooled followed by centrifugation (at 800 ***g*** for 10 min) to collect purified pachytene spermatocytes, round spermatids and elongating/elongated spermatids.

Development (2022) 149, dev199573. doi:10.1242/dev.199573

RNP and polysome fractionation

We fractionated the purified spermatogenic cells into RNP, monoribosome and polyribosome fractions using a continuous sucrose gradient ultracentrifugation method, as previously described (Zhang et al., 2017). In brief, a continuous sucrose gradient (15%-50%) was prepared by carefully overlaying 15% sucrose onto 50% sucrose followed by diffusing for 3 h at 4°C. The 15% and 50% sucrose solutions were prepared in a lysis buffer [containing 150 mM potassium acetate, 5 mM magnesium acetate, 2 mM DTT, protease inhibitor cocktail (Sigma-Aldrich, 1×), RNase inhibitor cocktail (Sigma-Aldrich, 1×), cycloheximide (100 ng/ml) and 50 mM HEPES, pH 7.5]. Freshly purified pachytene spermatocytes, round spermatids and elongating/elongated spermatids were homogenized in the lysis buffer freshly supplemented with 0.5% Triton X-100 and 0.25 M sucrose. The homogenates were centrifuged at ∼500 ***g*** for 15 min at 4°C to remove tissue debris, unbroken cells and nuclei. The supernatant was loaded onto the continuous 15-50% sucrose gradient followed by centrifugation at 150,000 ***g*** (35,000 rpm) for 3 h at 4°C. A tiny hole was punched gently at the bottom of the tubes for fraction collection. Twenty-four 500-µl fractions were collected followed by UV spectrometer measurement for OD_{254}.

Sperm purification

Both sides of epididymis were removed from adult C57/B6 mouse. Cauda were minced in 1 ml of pre-balanced TYH buffer (Easycheck, M2050). The mixture was incubated at 37°C, 5% CO_2 for 10 min. After the incubation, the mixture was transferred to a 15 ml falcon tube with 3 ml pre-warmed TYH buffer at 37°C, 5% CO_2 for 30 min. Swimming-up sperms were then collected by carefully aspirating 1 ml from the mixture followed by 10 min of centrifugation at 10,000 ***g***. After washing twice with PBS, sperm were resuspended in 1 ml of Cellbanker 2 (Zenoaq) and were transferred to −80°C for storage.

PAPA-seq

Total RNA from all samples (cell sample RIN>8, polysome sample RIN>8, RNP not applicable, sperm sample RIN>3) was centrifuged to discard inhibitor pellet. mRNA was purified using Dynabeads® mRNA Purification Kit (Life Technology) according to the manufacturer's instruction. mRNA was checked using a 2100 Bioanalyzer RNA picochip to ensure integrity. Qualified mRNA was denatured at 65°C, chilled on ice and then added to GTP-ITP mix (0.5 mM each; TriLink BioTechnologies) and 1× NEBuffer 2 (New England Biolabs), 2 U poly(U) polymerase and 40 U RNase inhibitor, followed by incubation at 37°C for 1 h. The mRNAs tailed with GTP and ITPs were then purified by 1.8× volumes RNA cleanup Ampure beads (A63987, Beckmann Coulter) and eluted in 10.5µl H_2O, followed by reverse transcription. Then 2µl 3' coding DNA sequence (CDS) primer (10 µM) (5′-AAGCAGTGGTATCAACGCAGAGTACNNNNNNCCCCCCCCCC-CCTTT-3′) was added into the purified GI-tailed mRNA and incubated at 72°C for 3 min, followed by cooling down to 42°C at the 0.1°C/s speed. Then a master mix containing iso-template switch oligo (5′-AAG-CAGTGGTATCAACGCAGAGTACATrGrG+G-3′, where +G indicates locked nucleotide), SSII superscript transcriptase, 1× first strand buffer, DTT, dNTP and RNase inhibitor was added. The reaction was incubated at 42°C for 90 min and stopped by incubating at 70°C for 10 min. The full-length mRNA library reaction was set up with the following reagents: 1× KAPA HiFi master mix, PCR primers (5′-AAGCAGTGGTATCAACG-CAGAGT-3′) and 10 µl of synthesized cDNA. The PCR conditions were as follows: initial denaturation at 95°C for 2 min, followed by 15-18 cycles of amplification (denaturation at 98°C for 20 s, annealing at 65°C for 15 s, and elongation at 72°C for 4 min) with a final elongation at 72°C for 7 min. The amplified library was then purified with 1× and 0.4× Ampure XP DNA Beads separately and resuspended in 42 µl H_2O. We diluted 1 µl of the equal mass mixed library 5× and 1 µl was checked on high sensitivity DNA chip (Agilent Technologies).

PacBio sequencing

The purified PCR libraries were submitted to the Genomics core facility of BGI Genomics for PacBio sequencing. Sequencing libraries were prepared using the PacBio Amplicon Template Preparation and Sequencing Protocol (PN 100-081-600) and the SMRTbell Template Prep Kit 1.0-SPv3 according to the manufacturer's guidelines. Sequencing on the Sequel was performed in Diffusion mode using the Sequel Binding and Internal Ctrl Kit 2.0. Every library was sequenced on one SMRT Cells 1M v.2.1 with a 1×1200 min movie. Circular consensus sequence (CCS) reads were generated within the SMRT Link browser 5.0 (minimum full pass of three and minimum predicted accuracy of 90).

RNA extraction, GI tailing, RT-PCR and qPCR

RNA from testes [both wild type and the miR-506 family KO (XW)] or fractions (RNP and polysome) were extracted using mirVana™ miRNA Isolation Kit (AM1560, Thermo Fisher Scientific) according to the manufacturer's instructions. To obtain the full-length poly(A) tail, 100 ng of RNA from testes or fractions was used for GI tailing. GI tailing was performed using 2 U poly(U) polymerase (M0337S, New England Biolabs) supplied with a final concentration of 1× first strand buffer (from SMARTScribe™ Reverse Transcriptase, 639538, Takara), 2 U/µl RNase inhibitor (M0314L, New England Biolabs) and GTP (10106399001, Sigma-Aldrich) and ITP (I0879, Sigma-Aldrich) mix (0.5 mM each) in a 10 µl reaction at 37°C for 1 h. Then 1 µl of reverse transcription (RT) primer 1 (10 µM) was added into the GI-tailed mix after GI tailing, and incubated at 72°C for 3 min. When the temperature reached 42°C, 9 µl of RT mix containing a final concentration of 1× first strand buffer, 1 mM DTT, 1 mM dNTP, 2 U/µl RNase inhibitor (M0314L, New England Biolabs), and 2.5 U/µl SMARTScribe Reverse Transcriptase was added into the mix and incubated at 42°C for 60 min, followed by deactivation at 70°C for 10 min.

PCR reactions were conducted using the GoTaq Green master mix (M7123, Promega). The PCR conditions were as follows: initial denaturation at 95°C for 2 min, followed by 35 cycles of amplification (denaturation at 95°C for 30 s, annealing at 55°C for 30 s, and elongation at 72°C for 2 min) with a final elongation at 72°C for 5 min. PCR amplification products were generated using two primers to determine the poly(A) length. A gene-specific forward primer (*Fmr1* 3′ UTR F2) designed upstream of the polyadenylation site and universal reverse primer (PCR primer 1) was used to generate a product that includes the poly(A) tails of the gene-of-interest. Finally, the PCR products are separated on agarose gels. The poly(A) tail lengths of the gene of interest are the sizes of poly(A) PCR-amplified products minus the calculated length of the gene-specific forward primer to the putative polyadenylation start site. qPCR was performed using Fast SYBR™ Green Master Mix (4385612, Thermo Fisher Scientific). The qPCR conditions were as follows: initial denaturation at 95°C for 10 min, followed by 40 cycles of amplification (denaturation at 95°C for 15 s, annealing and elongation at 60°C for 1 min). The relative RNA expression levels were normalized to *Gapdh* or *Actb*. The primers used for PCR and qPCR are listed in Table S2.

Western blot

Western blot was performed as previously described (Wang et al., 2020b). GAPDH was used as internal control. The antibodies used are as follows: anti-DDX4 antibody (1:800, ab27591, Abcam), anti-β-actin antibody (1:6000, ab27591, Affinity), anti-FMRP antibody (1:800, ab27455, Abcam), anti-GAPDH antibody (1:6000, G9545, Sigma-Aldrich).

Bioinformatic analyses of PAPA-seq data

Full-length isoforms detection

First, we used NCBI BLAST (version 2.2.28+ with parameters '-outfmt 7-word_size 5') to map 5′ and 3′ primers to CCS reads, then used in house Perl script to parse standard pairs of 5′ and 3′ primers to CCS reads as the full-length isoform. Next, we trimmed the primer sequence and reported the unique molecular identifier in each full-length isoform. Finally, each isoform was oriented from 5′ to 3′ end (Fig. S19).

Poly(A) tails detection

We developed a special modified sliding window algorithmic approach to accurately and error-tolerantly detect poly(A) tails. For example, for the poly(A) tail TCGAAATCAAGAAAAACAAAAAA, we listed all the windows without overlap (from 3′ to 5′: AAAAAA, AAAAAC, AAG, AAATC, TCG) and obtained the percentage of A in each window (100%, 83.33%, 66.66%, 60%, 0%), which were defined as the parameter w1. Then

Development (2022) 149, dev199573. doi:10.1242/dev.199573

using a sliding window starting from the 3′ end, we can get the percentage of A in the total window, defined as the parameter w2. Based on the parameters optimized and benchmarked against a set of manually annotated poly(A) tail estimated from UHRR datasets, the w1 and w2 parameters were set to w1≥50% and w2≥70%. As for the example above, we listed all the sliding regions (AAAAAA w1=100% w2=100%, AAAAACAAAAAA w1=83.33% w2=91.66%, AAGAAAAACAAAAAA w1=66.66% w2=80%, AAATCAAGAAAAACAAAAAA w1=60% w2=80%, TCGAAATCAAGAAAAACAAAAAA w1=0% w2=69.56%), so we can define the poly(A) as AAATCAAGAAAAACAAAAAA.

Quantification and gene assignment

After poly(A) tails detection and trimming, the remaining fraction of each isoform was mapped to the mm10 genome using GMAP (version 2018-05-30) with parameters '-f samse -n 0 –min-intronlength 9 –max-intronlength-middle 500000 –max-intron length-ends 10000 –trim-end-exons 12'. Then, using cDNA_Cupcake (https://github.com/Magdoll/cDNA_Cupcake) python script collapse_isoforms_by_sam.py to collapse all samples isoforms, based on collapsed output, we used in house Perl script to get the isoform expression quantity in each sample. After collapse, nonredundant isoforms were detected using cuffcompare (version v2.0.2) assigned to Ensemble mm10 annotation gene models.

Isoforms coding frame prediction and UTR detection

The CDS coding frame and UTR region were predicted using TransDecoder (Oakley et al., 2014) from the nonredundant isoforms. The predicted CDS were further confirmed using NR and Pfam databases.

In silico miRNA target prediction

Computational prediction of miRNA targets is a crucial initial step in identifying miRNA:mRNA target interactions for experimental validation. In order to find possible targets, miRanda and TargetScan were used. The intersection targets with appropriate filter conditions such as MFE scores were taken for further analysis. We used miRanda (John et al., 2004) (with parameters '-en -20 -strict') and TargetScan (Agarwal et al., 2015) (with default parameter) to get the target genes of miRNA, extracted intersection or union of the target genes as a final prediction result.

Statistical analyses

Both unpaired one-tailed Student's *t*-test and Wilcoxon rank sum test (a non-parametric or distribution-free test) were used for statistical analyses. The majority of the data followed a lognormal distribution. The Student's *t*-test was also performed on the logarithm data.

Competing interests

The authors declare no competing or financial interests.

Author contributions

Conceptualization: Q.G., Y.Z., F.S., W.Y., C.T.; Methodology: M.G., C.L., Z.W., D.M., F.R., Z.C., X.W., C.W., B.L., Z.L., Y.Z., C.T.; Validation: M.G., C.L., Z.W., S.C., D.M., F.R., Z.C., X.W., C.W., B.L., Z.L., J.H., D.Z., Y.Z.; Formal analysis: S.C., Z.C., W.Y.; Investigation: C.L., S.C., L.Y., X.W., D.Z., C.Y.; Resources: Z.W., S.C., C.Y., H.W., Y.Z., F.S.; Data curation: C.L., L.Y., C.T.; Writing - original draft: M.G., C.L., Z.W., F.S., W.Y., C.T.; Writing - review & editing: Z.W., S.C., F.R., Z.C., L.Y., X.W., Z.L., Y.Z., C.T.; Supervision: L.Y., J.H., C.Y., Q.G., H.W., F.S., W.Y., C.T.; Project administration: L.Y., J.H., C.Y., Q.G., H.W., C.T.; Funding acquisition: M.G., Q.G., H.W., Y.Z., F.S., W.Y.

Funding

This work was supported by grants from The National Key Research and Development Program of China (2021YFC2700200 and 2018YFC1003500 to F.S.), the Science, Technology, and Innovation Commission of Shenzhen Municipality (JSGG20170824152728492), National Natural Science Foundation of China (81801523 to Y.Z.; 81430027 and 81671510 to F.S.). The work on *Drosha* and X-linked miR-506 family KO mice was supported by grants from the National Institutes of Health (HD071736 and HD085506 to W.Y.) and the John Templeton Foundation (PID: 61174 to W.Y.). Deposited in PMC for release after 12 months.

Data availability

The original data of both large and small RNA-seq data have been deposited into the CNGB database under accession number CNP0001945. The code has been uploaded to GitHub (https://github.com/shizhuoxing/BGI-Full-Length-RNA-Analysis-Pipeline).

References

Agarwal, V., Bell, G. W., Nam, J.-W. and Bartel, D. P. (2015). Predicting effective microRNA target sites in mammalian mRNAs. *eLife* **4**, e05005. doi:10.7554/eLife.05005

Andreassi, C. and Riccio, A. (2009). To localize or not to localize: mRNA fate is in 3′UTR ends. *Trends Cell Biol.* **19**, 465-474. doi:10.1016/j.tcb.2009.06.001

Bao, J., Vitting-Seerup, K., Waage, J., Tang, C., Ge, Y., Porse, B. T. and Yan, W. (2016). UPF2-dependent nonsense-mediated mRNA decay pathway is essential for spermatogenesis by selectively eliminating longer 3′UTR transcripts. *PLoS Genet.* **12**, e1005863. doi:10.1371/journal.pgen.1005863

Bettegowda, A. and Smith, G. W. (2007). Mechanisms of maternal mRNA regulation: implications for mammalian early embryonic development. *Front. Biosci.* **12**, 3713-3726. doi:10.2741/2346

Bettegowda, A. and Wilkinson, M. F. (2010). Transcription and post-transcriptional regulation of spermatogenesis. *Philos. Trans. R. Soc. Lond. B Biol. Sci.* **365**, 1637-1651. doi:10.1098/rstb.2009.0196

Boehm, V., Haberman, N., Ottens, F., Ule, J. and Gehring, N. H. (2014). 3′ UTR length and messenger ribonucleoprotein composition determine endocleavage efficiencies at termination codons. *Cell Rep.* **9**, 555-568. doi:10.1016/j.celrep.2014.09.012

Braun, R. E. (1998). Post-transcriptional control of gene expression during spermatogenesis. *Semin. Cell Dev. Biol.* **9**, 483-489. doi:10.1006/scdb.1998.0226

Chang, H., Lim, J., Ha, M. and Kim, V. N. (2014). TAIL-seq: genome-wide determination of poly(A) tail length and 3′ end modifications. *Mol. Cell* **53**, 1044-1052. doi:10.1016/j.molcel.2014.02.007

Chen, C.-Y. A., Zheng, D., Xia, Z. and Shyu, A.-B. (2009). Ago–TNRC6 triggers microRNA-mediated decay by promoting two deadenylation steps. *Nat. Struct. Mol. Biol.* **16**, 1160-1166. doi:10.1038/nsmb.1709

Cui, X.-S. and Kim, N.-H. (2007). Maternally derived transcripts: identification and characterisation during oocyte maturation and early cleavage. *Reprod. Fertil. Dev.* **19**, 25-34. doi:10.1071/RD06128

Curinha, A., Oliveira Braz, S., Pereira-Castro, I., Cruz, A. and Moreira, A. (2014). Implications of polyadenylation in health and disease. *Nucleus* **5**, 508-519. doi:10.4161/nucl.36360

Di Giammartino, D. C., Nishida, K. and Manley, J. L. (2011). Mechanisms and consequences of alternative polyadenylation. *Mol. Cell* **43**, 853-866. doi:10.1016/j.molcel.2011.08.017

Eichhorn, S. W., Subtelny, A. O., Kronja, I., Kwasnieski, J. C., Orr-Weaver, T. L. and Bartel, D. P. (2016). mRNA poly(A)-tail changes specified by deadenylation broadly reshape translation in Drosophila oocytes and early embryos. *eLife* **5**, e16955. doi:10.7554/eLife.16955

Elkon, R., Ugalde, A. P. and Agami, R. (2013). Alternative cleavage and polyadenylation: extent, regulation and function. *Nat. Rev. Genet.* **14**, 496-506. doi:10.1038/nrg3482

Eulalio, A., Huntzinger, E., Nishihara, T., Rehwinkel, J., Fauser, M. and Izaurralde, E. (2009). Deadenylation is a widespread effect of miRNA regulation. *RNA* **15**, 21-32. doi:10.1261/rna.1399509

Fabian, M. R., Cieplak, M. K., Frank, F., Morita, M., Green, J., Srikumar, T., Nagar, B., Yamamoto, T., Raught, B., Duchaine, T. F. et al. (2011). miRNA-mediated deadenylation is orchestrated by GW182 through two conserved motifs that interact with CCR4-NOT. *Nat. Struct. Mol. Biol.* **18**, 1211-1217. doi:10.1038/nsmb.2149

Flamand, M. N., Wu, E., Vashisht, A., Jannot, G., Keiper, B. D., Simard, M. J., Wohlschlegel, J. and Duchaine, T. F. (2016). Poly(A)-binding proteins are required for microRNA-mediated silencing and to promote target deadenylation in C. elegans. *Nucleic Acids Res.* **44**, 5924-5935. doi:10.1093/nar/gkw276

Gohin, M., Fournier, E., Dufort, I. and Sirard, M.-A. (2014). Discovery, identification and sequence analysis of RNAs selected for very short or long poly A tail in immature bovine oocytes. *Mol. Hum. Reprod.* **20**, 127-138. doi:10.1093/molehr/gat080

Goldstrohm, A. C. and Wickens, M. (2008). Multifunctional deadenylase complexes diversify mRNA control. *Nat. Rev. Mol. Cell Biol.* **9**, 337-344. doi:10.1038/nrm2370

Han, J., Lee, Y., Yeom, K. H., Nam, J. W., Heo, I., Rhee, J. K., Sohn, S. Y., Cho, Y., Zhang, B. T. and Kim, V. N. (2006). Molecular basis for the recognition of primary microRNAs by the Drosha-DGCR8 complex. *Cell* **125**, 887-901. doi:10.1016/j.cell.2006.03.043

Hermo, L., Pelletier, R.-M., Cyr, D. G. and Smith, C. E. (2010). Surfing the wave, cycle, life history, and genes/proteins expressed by testicular germ cells. Part 2: changes in spermatid organelles associated with development of spermatozoa. *Microsc. Res. Tech.* **73**, 279-319. doi:10.1002/jemt.20787

Hilgers, V. (2015). Alternative polyadenylation coupled to transcription initiation: Insights from ELAV-mediated 3′ UTR extension. *RNA Biol.* **12**, 918-921. doi:10.1080/15476286.2015.1060393
Hofweber, M. and Dormann, D. (2019). Friend or foe-Post-translational modifications as regulators of phase separation and RNP granule dynamics. *J. Biol. Chem.* **294**, 7137-7150. doi:10.1074/jbc.TM118.001189
Idler, R. K. and Yan, W. (2012). Control of messenger RNA fate by RNA-binding proteins: an emphasis on mammalian spermatogenesis. *J. Androl.* **33**, 309-337. doi:10.2164/jandrol.111.014167
Iguchi, N., Tobias, J. W. and Hecht, N. B. (2006). Expression profiling reveals meiotic male germ cell mRNAs that are translationally up- and down-regulated. *Proc. Natl. Acad. Sci. USA* **103**, 7712-7717. doi:10.1073/pnas.0510999103
Ivshina, M., Lasko, P. and Richter, J. D. (2014). Cytoplasmic polyadenylation element binding proteins in development, health, and disease. *Annu. Rev. Cell Dev. Biol.* **30**, 393-415. doi:10.1146/annurev-cellbio-101011-155831
Jia, J., Yao, P., Arif, A. and Fox, P. L. (2013). Regulation and dysregulation of 3′ UTR-mediated translational control. *Curr. Opin. Genet. Dev.* **23**, 29-34. doi:10.1016/j.gde.2012.12.004
John, B., Enright, A. J., Aravin, A., Tuschl, T., Sander, C. and Marks, D. S. (2004). Human MicroRNA targets. *PLoS Biol.* **2**, e363. doi:10.1371/journal.pbio.0020363
Kashiwabara, S.-I., Noguchi, J., Zhuang, T., Ohmura, K., Honda, A., Sugiura, S., Miyamoto, K., Takahashi, S., Inoue, K., Ogura, A. et al. (2002). Regulation of spermatogenesis by testis-specific, cytoplasmic Poly(A) Polymerase TPAP. *Science (New York, N.Y.)***298**, 1999-2002. doi:10.1126/science.1074632
Kashiwabara, S., Nakanishi, T., Kimura, M. and Baba, T. (2008). Non-canonical poly(A) polymerase in mammalian gametogenesis. *Biochim. Biophys. Acta* **1779**, 230-238.
Kashiwabara, S.-I., Tsuruta, S., Okada, K., Yamaoka, Y. and Baba, T. (2016). Adenylation by testis-specific cytoplasmic poly(A) polymerase, PAPOLB/TPAP, is essential for spermatogenesis. *J. Reprod. Dev.* **62**, 607-614. doi:10.1262/jrd.2016-116
Keeling, K. M., Salas-Marco, J., Osherovich, L. Z. and Bedwell, D. M. (2006). Tpa1p is part of an mRNP complex that influences translation termination, mRNA deadenylation, and mRNA turnover in Saccharomyces cerevisiae. *Mol. Cell. Biol.* **26**, 5237-5248. doi:10.1128/MCB.02448-05
Keene, J. D. (2007). RNA regulons: coordination of post-transcriptional events. *Nat. Rev. Genet.* **8**, 533-543. doi:10.1038/nrg2111
Kim, H. K. (2019). Transfer RNA-derived small non-coding RNA: dual regulator of protein synthesis. *Mol. Cells* **42**, 687-692.
Kleene, K. C. (1989). Poly(A) shortening accompanies the activation of translation of five mRNAs during spermiogenesis in the mouse. *Development* **106**, 367-373. doi:10.1242/dev.106.2.367
Kleene, K., Distel, R. J. and Hecht, N. B. (1984). Translational regulation and deadenylation of a protamine mRNA during spermiogenesis in the mouse. *Dev. Biol.* **105**, 71-79. doi:10.1016/0012-1606(84)90262-8
Kleene, K. C., Wang, M. Y., Cutler, M., Hall, C. and Shih, D. (1994). Developmental expression of poly(A) binding protein mRNAs during spermatogenesis in the mouse. *Mol. Reprod. Dev.* **39**, 355-364. doi:10.1002/mrd.1080390403
Kotaja, N. and Sassone-Corsi, P. (2007). The chromatoid body: a germ-cell-specific RNA-processing centre. *Nat. Rev. Mol. Cell Biol.* **8**, 85-90. doi:10.1038/nrm2081
Kotaja, N., Lin, H., Parvinen, M. and Sassone-Corsi, P. (2006). Interplay of PIWI/Argonaute protein MIWI and kinesin KIF17b in chromatoid bodies of male germ cells. *J. Cell Sci.* **119**, 2819-2825. doi:10.1242/jcs.03022
Kusov, Y. Y., Shatirishvili, G., Dzagurov, G. and Gauss-Müller, V. (2001). A new G-tailing method for the determination of the poly(A) tail length applied to hepatitis A virus RNA. *Nucleic Acids Res.* **29**, e57. doi:10.1093/nar/29.12.e57
Legnini, I., Alles, J., Karaiskos, N., Ayoub, S. and Rajewsky, N. (2019). FLAM-seq: full-length mRNA sequencing reveals principles of poly(A) tail length control. *Nat. Methods* **16**, 879-886. doi:10.1038/s41592-019-0503-y
Lim, J., Lee, M., Son, A., Chang, H. and Kim, V. N. (2016). mTAIL-seq reveals dynamic poly(A) tail regulation in oocyte-to-embryo development. *Genes Dev.* **30**, 1671-1682. doi:10.1101/gad.284802.116
Liu, Y., Nie, H., Liu, H. and Lu, F. (2019). Poly(A) inclusive RNA isoform sequencing (PAIso-seq) reveals wide-spread non-adenosine residues within RNA poly(A) tails. *Nat. Commun.* **10**, 5292. doi:10.1038/s41467-019-13228-9
Lunde, B. M., Moore, C. and Varani, G. (2007). RNA-binding proteins: modular design for efficient function. *Nat. Rev. Mol. Cell Biol.* **8**, 479-490. doi:10.1038/nrm2178
Matsui, M., Horiguchi, H., Kamma, H., Fujiwara, M., Ohtsubo, R. and Ogata, T. (2000). Testis- and developmental stage-specific expression of hnRNP A2/B1 splicing isoforms, B0a/b. *Biochim. Biophys. Acta* **1493**, 33-40. doi:10.1016/S0167-4781(00)00154-8
Mayr, C. (2017). Regulation by 3'-Untranslated Regions. *Annu. Rev. Genet.* **51**, 171-194. doi:10.1146/annurev-genet-120116-024704
Meikar, O., Da Ros, M., Korhonen, H. and Kotaja, N. (2011). Chromatoid body and small RNAs in male germ cells. *Reproduction (Cambridge, England)* **142**, 195-209. doi:10.1530/REP-11-0057
Morgan, M., Much, C., DiGiacomo, M., Azzi, C., Ivanova, I., Vitsios, D. M., Pistolic, J., Collier, P., Moreira, P. N., Benes, V. et al. (2017). mRNA 3′ uridylation and poly(A) tail length sculpt the mammalian maternal transcriptome. *Nature* **548**, 347-351. doi:10.1038/nature23318
Morgan, M., Kabayama, Y., Much, C., Ivanova, I., Di Giacomo, M., Auchynnikava, T., Monahan, J. M., Vitsios, D. M., Vasiliauskaite, L., Comazzetto, S. et al. (2019). A programmed wave of uridylation-primed mRNA degradation is essential for meiotic progression and mammalian spermatogenesis. *Cell Res.* **29**, 221-232. doi:10.1038/s41422-018-0128-1
Moser, J. J. and Fritzler, M. J. (2010). Cytoplasmic ribonucleoprotein (RNP) bodies and their relationship to GW/P bodies. *Int. J. Biochem. Cell Biol.* **42**, 828-843. doi:10.1016/j.biocel.2009.11.018
Moser, J. J. and Fritzler, M. J. (2013). Relationship of other cytoplasmic ribonucleoprotein bodies (cRNPB) to GW/P bodies. *Adv. Exp. Med. Biol.* **768**, 213-242. doi:10.1007/978-1-4614-5107-5_13
Nicholson, A. L. and Pasquinelli, A. E. (2019). Tales of Detailed Poly(A) Tails. *Trends Cell Biol.* **29**, 191-200. doi:10.1016/j.tcb.2018.11.002
Norbury, C. J. (2013). Cytoplasmic RNA: a case of the tail wagging the dog. *Nat. Rev. Mol. Cell Biol.* **14**, 643-653. doi:10.1038/nrm3645
Oakley, T. H., Alexandrou, M. A., Ngo, R., Pankey, M. S., Churchill, C. K. C., Chen, W. and Lopker, K. B. (2014). Osiris: accessible and reproducible phylogenetic and phylogenomic analyses within the Galaxy workflow management system. *BMC Bioinformatics* **15**, 230. doi:10.1186/1471-2105-15-230
Ostareck-Lederer, A. and Ostareck, D. H. (2012). Precision mechanics with multifunctional tools: how hnRNP K and hnRNPs E1/E2 contribute to post-transcriptional control of gene expression in hematopoiesis. *Curr. Protein Pept. Sci.* **13**, 391-400. doi:10.2174/138920312801619484
Peruquetti, R. L. (2015). Perspectives on mammalian chromatoid body research. *Anim. Reprod. Sci.* **159**, 8-16. doi:10.1016/j.anireprosci.2015.05.018
Piccolo, L. L., Corona, D. and Onorati, M. C. (2014). Emerging roles for hnRNPs in post-transcriptional regulation: what can we learn from flies? *Chromosoma* **123**, 515-527. doi:10.1007/s00412-014-0470-0
Ramaiah, M., Tan, K., Plank, T. D. M., Song, H. W., Dumdie, J. N., Jones, S., Shum, E. Y., Sheridan, S. D., Peterson, K. J., Gromoll, J. et al. (2019). A microRNA cluster in the Fragile-X region expressed during spermatogenesis targets FMR1. *EMBO Rep.* **20**, e46566. doi:10.15252/embr.201846566
Richter, J. D. (1999). Cytoplasmic polyadenylation in development and beyond. *Microbiol. Mol. Biol. Rev.* **63**, 446-456. doi:10.1128/MMBR.63.2.446-456.1999
Richter, J. D. (2001). Think globally, translate locally: what mitotic spindles and neuronal synapses have in common. *Proc. Natl. Acad. Sci. USA* **98**, 7069-7071. doi:10.1073/pnas.111146498
Sha, Q.-Q., Zhang, J. and Fan, H.-Y. (2019). A story of birth and death: mRNA translation and clearance at the onset of maternal-to-zygotic transition in mammals. *Biol. Reprod.* **101**, 579-590. doi:10.1093/biolre/ioz012
Shyu, A.-B., Wilkinson, M. F. and van Hoof, A. (2008). Messenger RNA regulation: to translate or to degrade. *EMBO J.* **27**, 471-481. doi:10.1038/sj.emboj.7601977
Subtelny, A. O., Eichhorn, S. W., Chen, G. R., Sive, H. and Bartel, D. P. (2014). Poly(A)-tail profiling reveals an embryonic switch in translational control. *Nature* **508**, 66-71. doi:10.1038/nature13007
Tang, C., Klukovich, R., Peng, H., Wang, Z., Yu, T., Zhang, Y., Zheng, H., Klungland, A. and Yan, W. (2018). ALKBH5-dependent m6A demethylation controls splicing and stability of long 3′-UTR mRNAs in male germ cells. *Proc. Natl. Acad. Sci. USA* **115**, E325-E333. doi:10.1073/pnas.1717794115
Tang, C., Xie, Y., Yu, T., Liu, N., Wang, Z., Woolsey, R. J., Tang, Y., Zhang, X., Qin, W., Zhang, Y. et al. (2020). m(6)A-dependent biogenesis of circular RNAs in male germ cells. *Cell Res.* **30**, 211-228. doi:10.1038/s41422-020-0279-8
Vasileva, A., Tiedau, D., Firooznia, A., Müller-Reichert, T. and Jessberger, R. (2009). Tdrd6 is required for spermiogenesis, chromatoid body architecture, and regulation of miRNA expression. *Curr. Biol.* **19**, 630-639. doi:10.1016/j.cub.2009.02.047
Vourekas, A., Zheng, Q., Alexiou, P., Maragkakis, M., Kirino, Y., Gregory, B. D. and Mourelatos, Z. (2012). Mili and Miwi target RNA repertoire reveals piRNA biogenesis and function of Miwi in spermiogenesis. *Nat. Struct. Mol. Biol.* **19**, 773-781. doi:10.1038/nsmb.2347
Wang, Z., Wang, Y., Wang, S., Gorzalski, A. J., McSwiggin, H., Yu, T., Castaneda-Garcia, K., Prince, B., Wang, H., Zheng, H. et al. (2020a). Efficient genome editing by CRISPR-Mb3Cas12a in mice. *J. Cell Sci.* **133**, jcs240705. doi:10.1242/jcs.240705
Wang, Z., Xie, Y., Wang, Y., Morris, D., Wang, S., Oliver, D., Yuan, S., Zayac, K., Bloomquist, S., Zheng, H. et al. (2020b). X-linked miR-506 family miRNAs promote FMRP expression in mouse spermatogonia. *EMBO Rep.* **21**, e49024. doi:10.15252/embr.201949024
Wormington, M. (1994). Unmasking the role of the 3′ UTR in the cytoplasmic polyadenylation and translational regulation of maternal mRNAs. *BioEssays* **16**, 533-535. doi:10.1002/bies.950160804
Wu, Q., Song, R., Ortogero, N., Zheng, H., Evanoff, R., Small, C. L., Griswold, M. D., Namekawa, S. H., Royo, H., Turner, J. M. et al. (2012).

The RNase III enzyme DROSHA is essential for microRNA production and spermatogenesis. *J. Biol. Chem.* **287**, 25173-25190. doi:10.1074/jbc.M112.362053

Yanagiya, A., Delbes, G., Svitkin, Y. V., Robaire, B. and Sonenberg, N. (2010). The poly(A)-binding protein partner Paip2a controls translation during late spermiogenesis in mice. *J. Clin. Invest.* **120**, 3389-3400. doi:10.1172/JCI43350

Yi, H., Park, J., Ha, M., Lim, J., Chang, H. and Kim, V. N. (2018). PABP cooperates with the CCR4-NOT complex to promote mRNA deadenylation and block precocious decay. *Mol. Cell* **70**(6), 1081-1088.e5. doi:10.1016/j.molcel.2018.05.009

Yuan, S., Stratton, C. J., Bao, J., Zheng, H., Bhetwal, B. P., Yanagimachi, R. and Yan, W. (2015). Spata6 is required for normal assembly of the sperm connecting piece and tight head-tail conjunction. *Proc. Natl. Acad. Sci. USA* **112**, E430-E439. doi:10.1073/pnas.1424648112

Zhang, Y., Tang, C., Yu, T., Zhang, R., Zheng, H. and Yan, W. (2017). MicroRNAs control mRNA fate by compartmentalization based on 3′ UTR length in male germ cells. *Genome Biol.* **18**, 105. doi:10.1186/s13059-017-1243-x

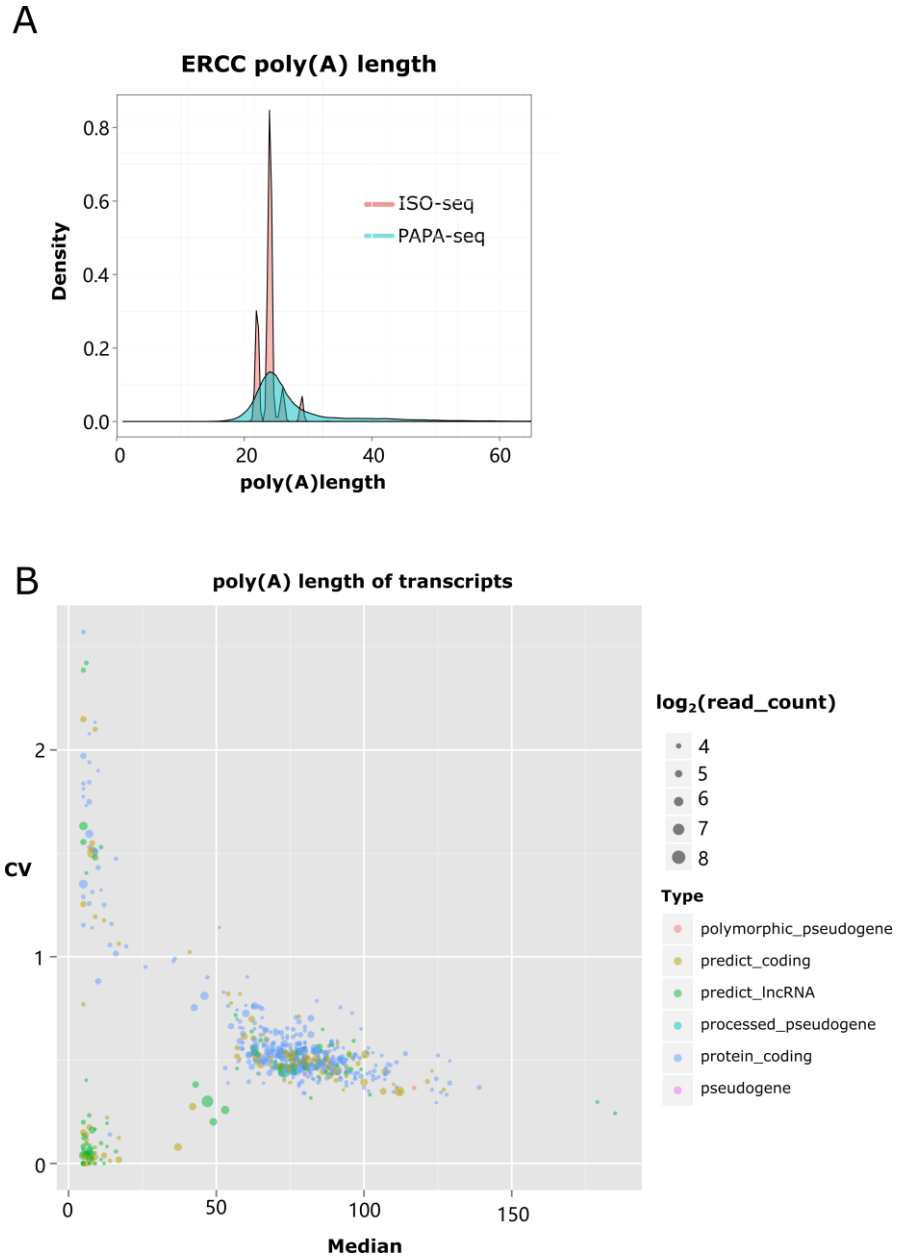

Fig. S1. Validation of PAPA-seq method and correlation between poly(A) tail length and coding potential. (A) Density plots showing that the PAPA-seq results are in line with the documented poly(A) lengths of ERCC spike-in references. ERCC contains synthetic RNAs with poly(A) tails of different lengths as spike-in references. The deviation is 5.8nt in poly(A) tail length measurement. (B) Scattered plots showing no significant correlation between poly(A) tail length and coding potential. The x-axis represents the median poly(A) length values, while the y-axis shows the coefficient of variation. pseudogene: genes that have homology to proteins but generally suffer from a disrupted coding sequence, and an active homologous gene can be found at another locus. processed_pseudogene: pseudogene that lacks introns and is thought to arise from reverse transcription of mRNA followed by reinsertion of DNA into the genome. polymorphic_pseudogene: pseudogene owing to an SNP/DIP, but in other individuals/haplotypes/strains, the gene is translated. protein_coding: genes that contain a documented open reading frame (ORF). predicted _coding: genes that have software predicted coding potential. predicted_lncRNA: genes predicted to be noncoding genes by software. Data were from samples of one biological replicate and two technical replicates.

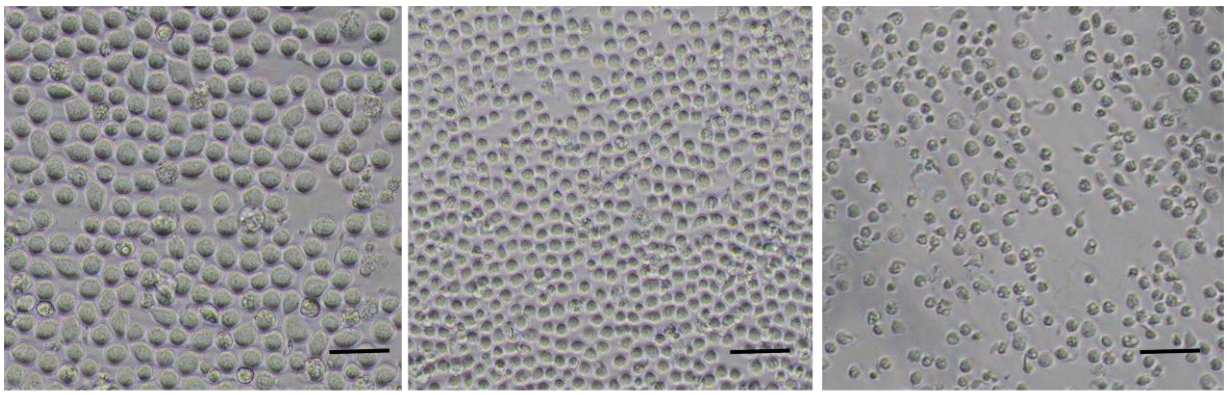

Fig. S2. Purity of cells. Using a modified STA-PUT method, pachytene spermatocytes, round and elongating spermatids were purified from adult mouse testes for isolation of RNA. The purity for the three cell types (pachytene spermatocytes, round and elongating spermatids) was determined to be 90%, 90% and 75%, respectively. Scale bar=20µm.

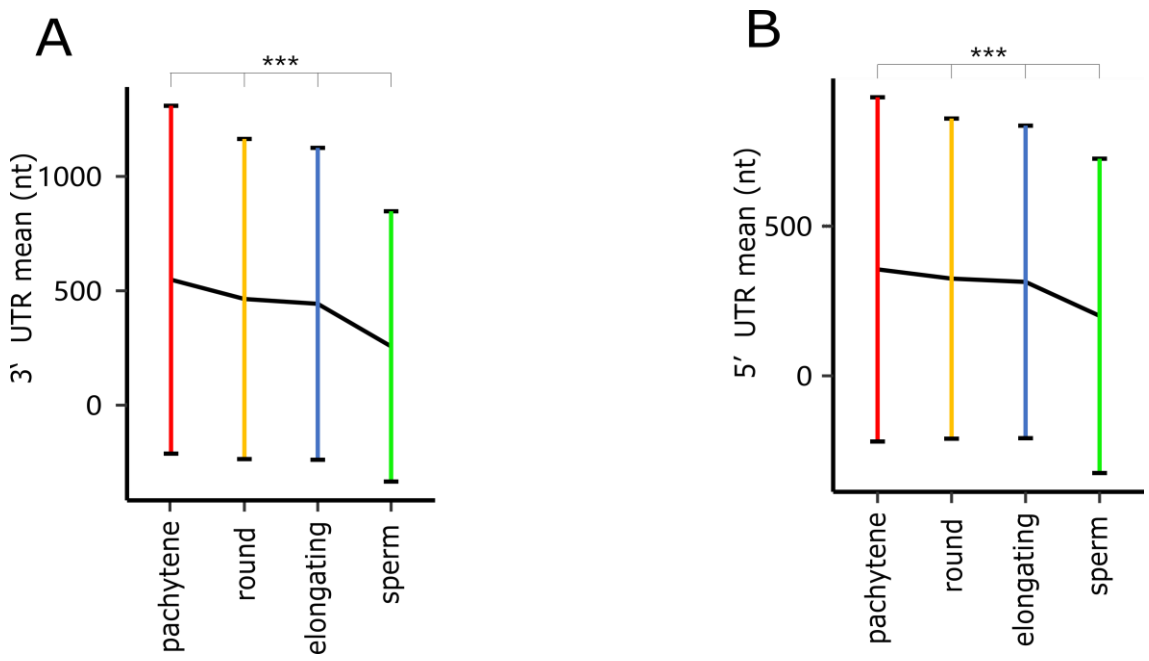

Fig. S3. Changes in 3' and 5' UTR length in three male germ cell types during spermatogenesis. (A) Line plots showing the average 3'UTR lengths in pachytene spermatocytes, round spermatids, elongating spermatids and spermatozoa. (B) Line plots showing the 3'UTR length distribution in pachytene spermatocytes, round spermatids, elongating spermatids and spermatozoa. *: p< 0.1,**: p< 0.05, ***: p< 0.01, log t-test. Data were based on samples from two independent preparations with 3-6 mice in each, plus two technical replicates.

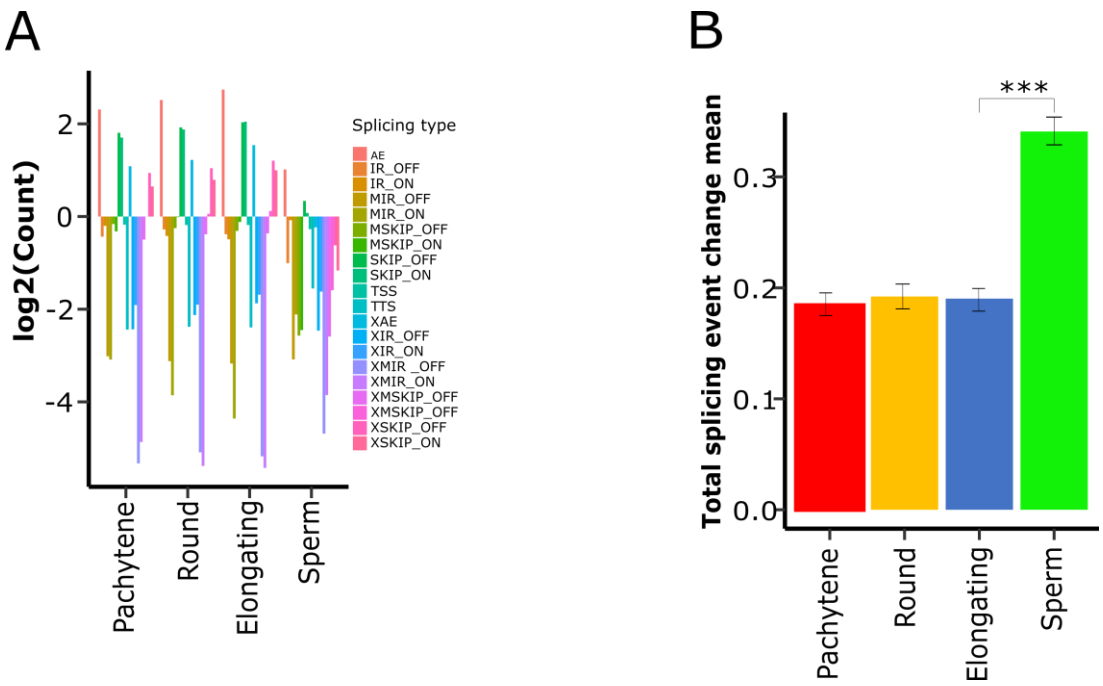

Fig. S4. Patterns of splicing events in three male germ cell types during spermatogenesis. (A) Distribution of various individual splicing types in the pachytene spermatocytes, round spermatids, elongating spermatids and spermatozoa, including exon skipping (SKIP), multiple exons skipping (MSKIP), alternative transcript start and termination (TSS, TTS), retention of single (IR) or multiple (MIR) introns, and alternative exon ends (AE). SKIP means single exon skipping. MSKIP means multiple exons skipping. (B) The average splicing events of all the genes in the pachytene spermatocytes, round spermatids, elongating spermatids and spermatozoa. (*: p< 0.1,**: p< 0.05, ***: p< 0.01, Wilcoxon rank test. Data were based on samples from two independent preparations with 3-6 mice in each, plus two technical replicates.

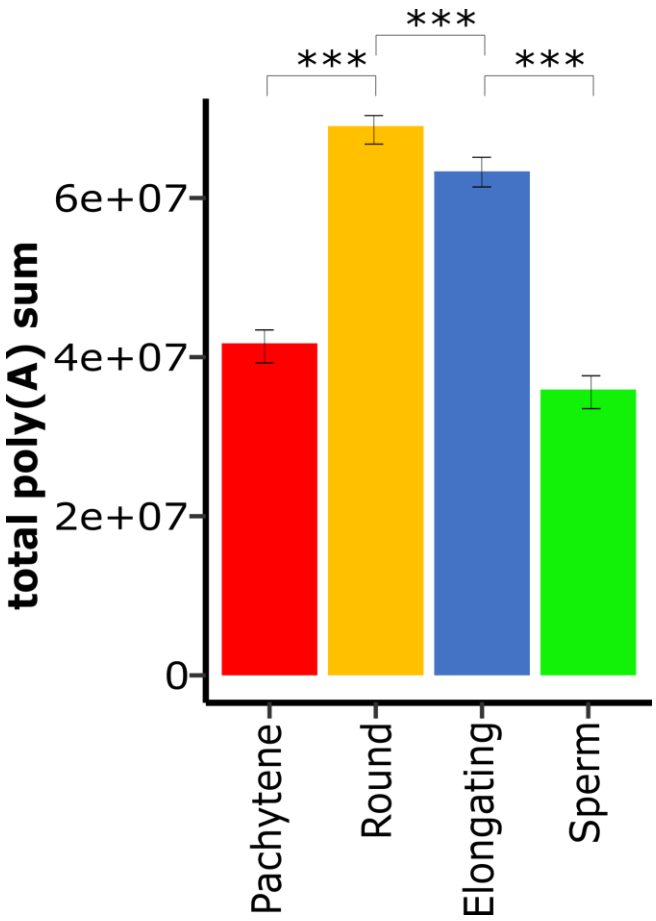

Fig. S5. Total counts of adenine in all transcripts in spermatogenic cells during spermatogenesis. All of adenine nucleotides in all the transcripts were counted and plotted to reflect polyadenylation activity, which appears to the highest in the round and elongating spermatids. (*: p< 0.1,**: p< 0.05, ***: p< 0.01, log t-test. Data were based on samples from two independent preparations with 3-6 mice in each, plus two technical replicates.

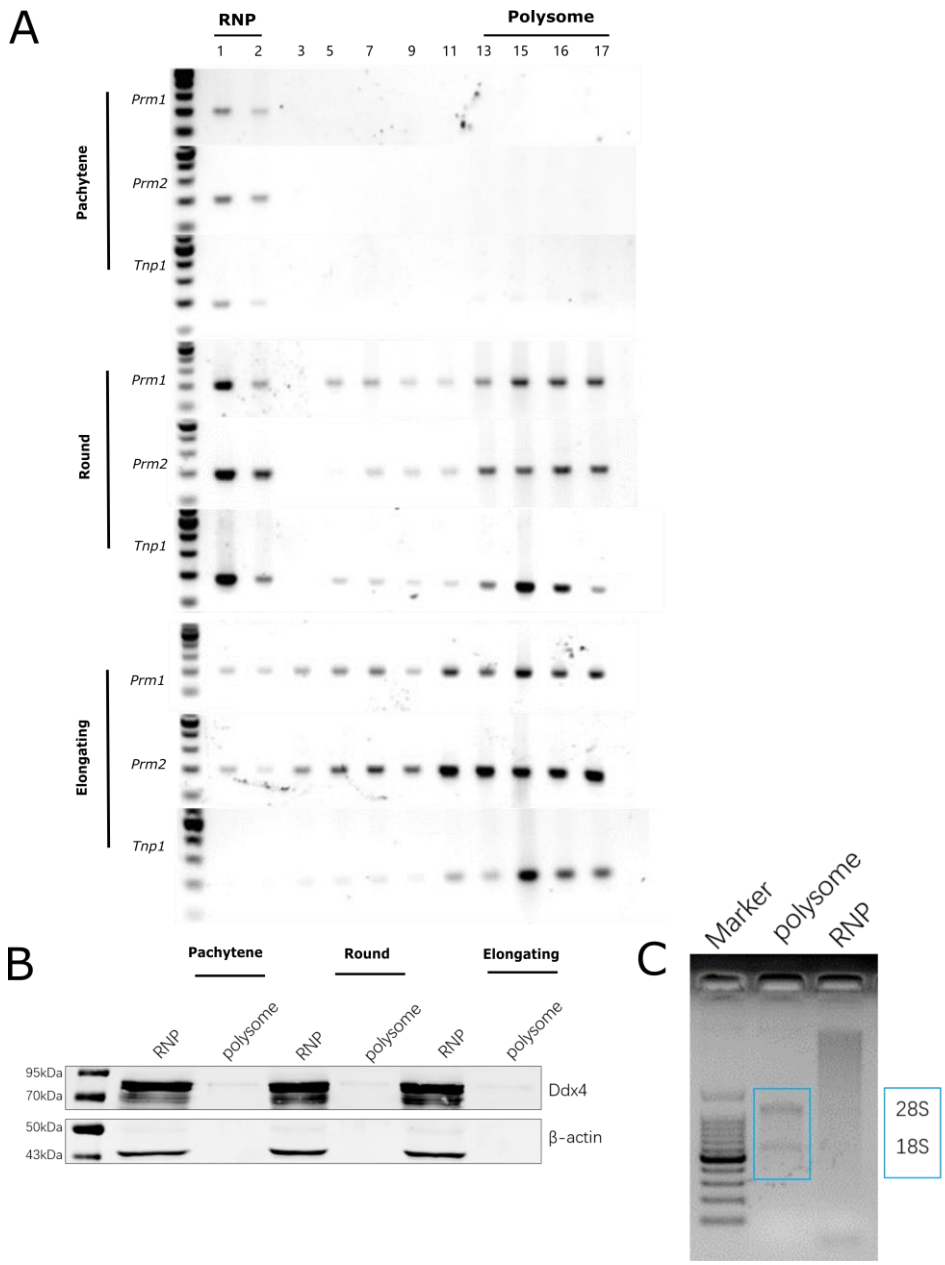

Fig. S6. Determining the purity of the fractions by PCR and western. (A) *Prm1*, *Prm2*, and *Tnp1* are well-known delayed translational genes in testis. mRNAs for these genes are located in RNP fractions of pachytene spermatocytes and gradually translocated to polysome fractions of round spermatids. mRNA for these genes were used as marker genes to identify the fraction purity. The semi-quantitative PCR results of fractions showed the fraction purity. (B) Ddx4 is one of the most important components in the nuages. We used Ddx4 as co-localization maker to determine the RNP fraction, which showed that the nuage was found in the top most fractions by western analysis. (C) RNA distribution in polysome and RNP fractions.

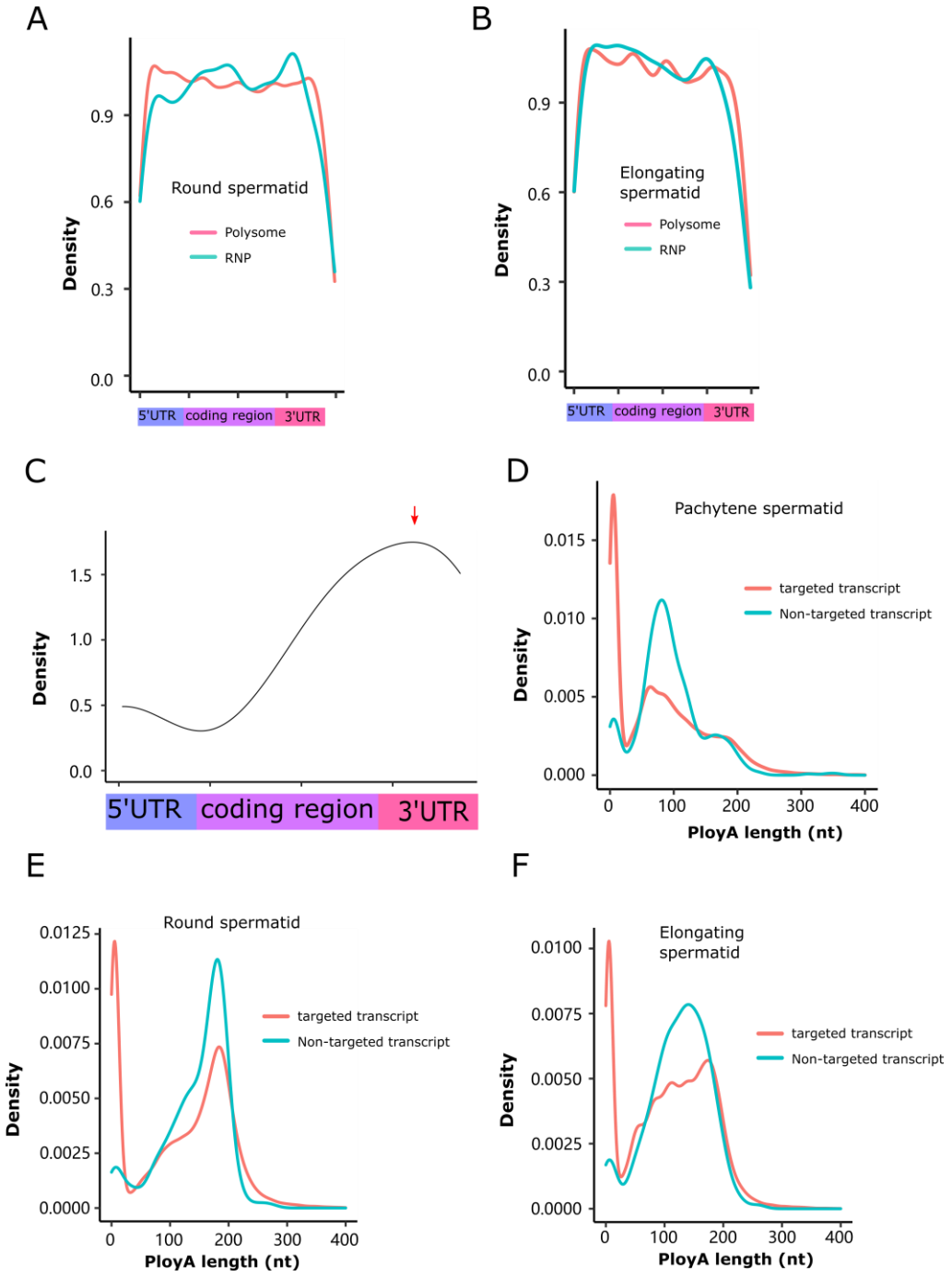

Fig. S7. miRNA target site distribution. (A) The miRNA targeted site distribution along transcripts in round spermatids. The green lines indicated the RNP enriched miRNAs and red lines indicated the polysome enriched miRNAs. (B) The miRNA targeted site distribution along transcripts in elongating spermatids. (C) The miRNA targeted site distribution along Spata6 transcripts indicated the miRNA targeted position is conserved in the 3'UTR. (D-F) The poly(A) length distribution of predicted miR-34 targeted transcripts and non-targeted transcripts in three spermatogenic cell types during spermatogenesis.

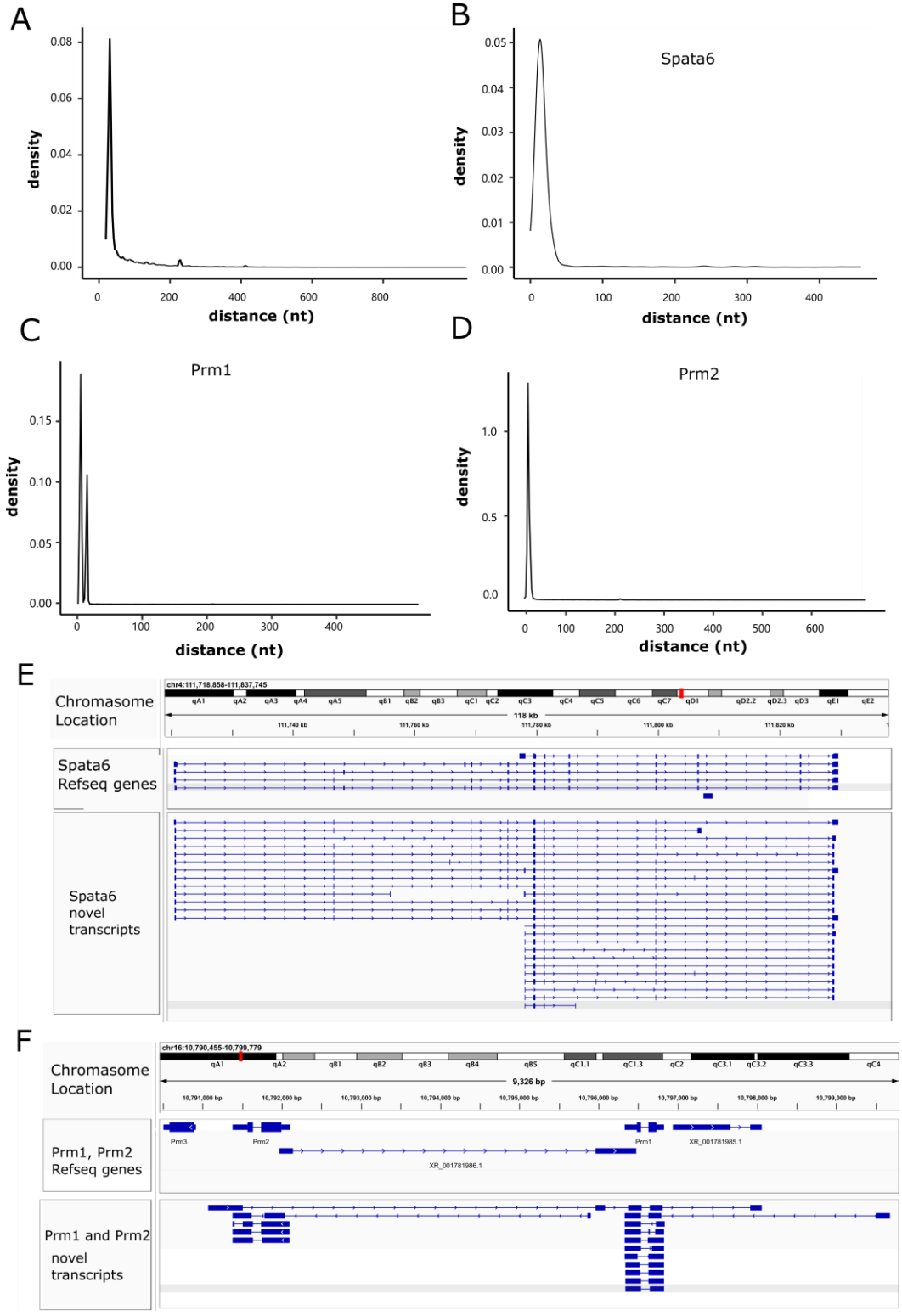

Fig. S8. Analyses of alternative polyadenylation site and novel isoforms *of Spata6*, *Prm1* and *Prm2*. The x-axis demonstrated the distance between the alternative polyadenylation motif and 3'end. The result of all transcripts (A), *Spata6* (B) and *Prm1*and *Prm2* (C and D) suggested that most of the transcripts in RNPs use the distal alternative polyadenylation motif (more toward the 3' end). (E-F) Schematic grams of novel transcripts of Spata6 (E) and Prm1 and 2 (F) in the fraction of polysome. Dark blue vertical solid lines stand for exons. Line with arrows means introns.

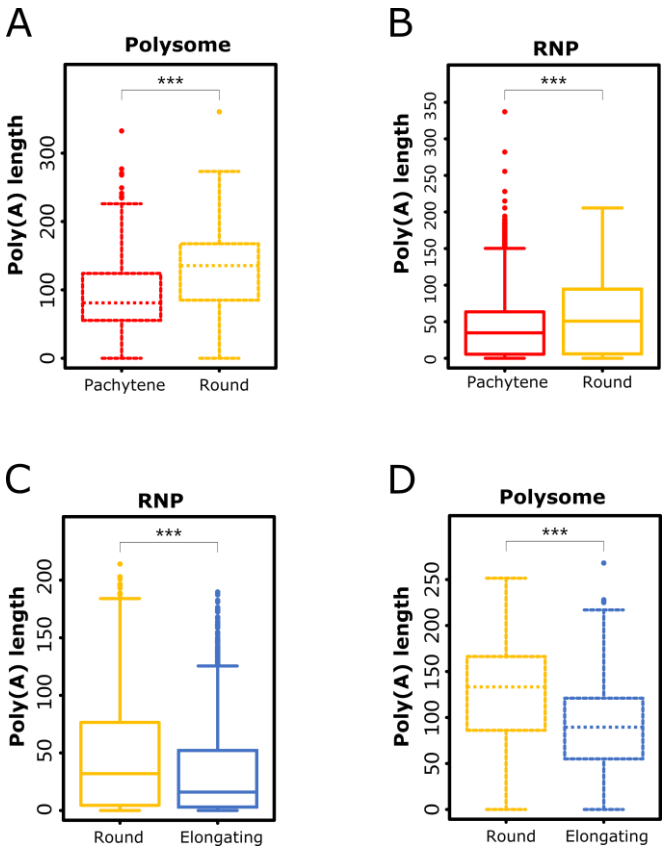

Fig. S9. Comparison of poly(A) length in RNP and polysome fractions in three spermatogenic cell types during spermatogenesis.

(A) Box plots showing the poly(A) length distribution in polysome fractions between pachytene spermatocytes and round spermatids. The poly(A) length in the polysome fractions of round spermatids is ~1.5x longer than that in pachytene spermatocytes. (B) Box plots showing the poly(A) length distribution in the RNP fractions between pachytene spermatocytes and round spermatids. The poly(A) length in RNPs of round spermatids is ~1.4x longer than that in pachytene spermatocytes. (C) Box plots showing the poly(A) length distribution in RNP fractions between round spermatids and elongating spermatids. The poly(A) length in RNPs of the round spermatids is ~2x longer than that in elongating spermatids. (D) Box plots showing the poly(A) length distribution in polysome fractions between round spermatids and elongating spermatids. The poly(A) length in polysome fractions of the round spermatids is ~1.5x longer than in the elongating spermatids.

(*: $p < 0.1$,**: $p < 0.05$, ***: $p < 0.01$, log t-test. Data were based on samples from two independent preparations with 3-6 mice in each, plus two technical replicates.

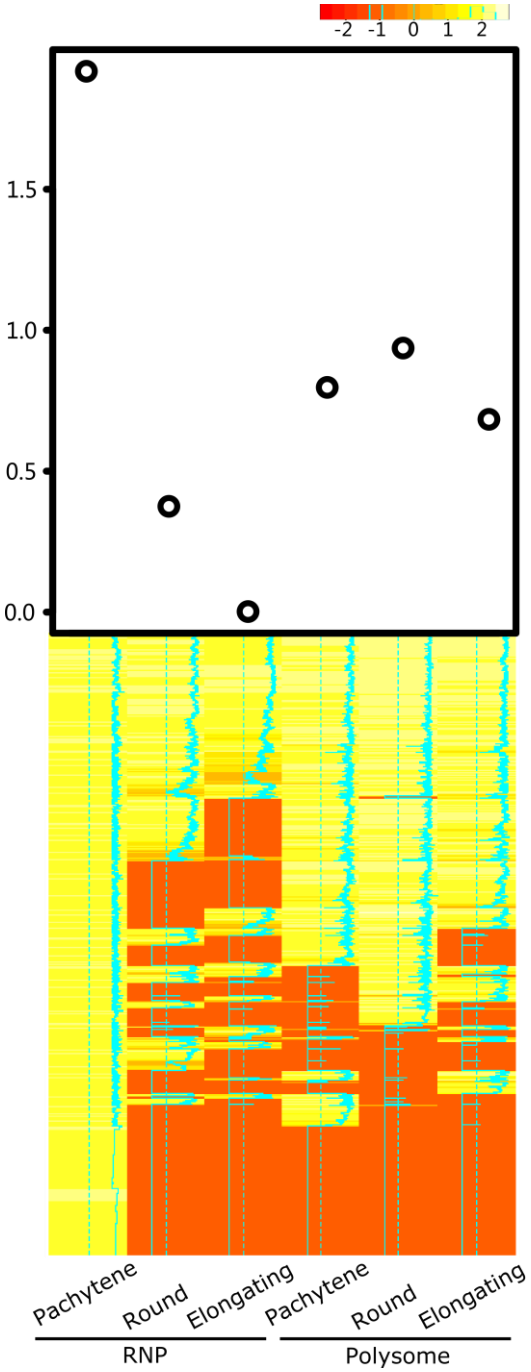

Fig. S10. Dynamic changes in ploy(A) length among the transcripts with longer poly(A) tails (>50nt) in RNP granules of pachytene spermatocytes. The poly(A) tails of RNP enriched transcripts were shortened from pachytene spermatocytes to elongating spermatids. In contrast, the poly(A) tails of polysome enriched transcripts were elongated in the progress. The upper panel showed the average poly(A) length in each fraction. The Y axis means the log value of poly(A) length. The color bar means mRNA poly(A) length. The color bar is scaled by the Z-score. Green lines running in the center of heatmaps mean the value of Z-scores. Data were based on samples from two independent preparations with 3-6 mice in each, plus two technical replicates.

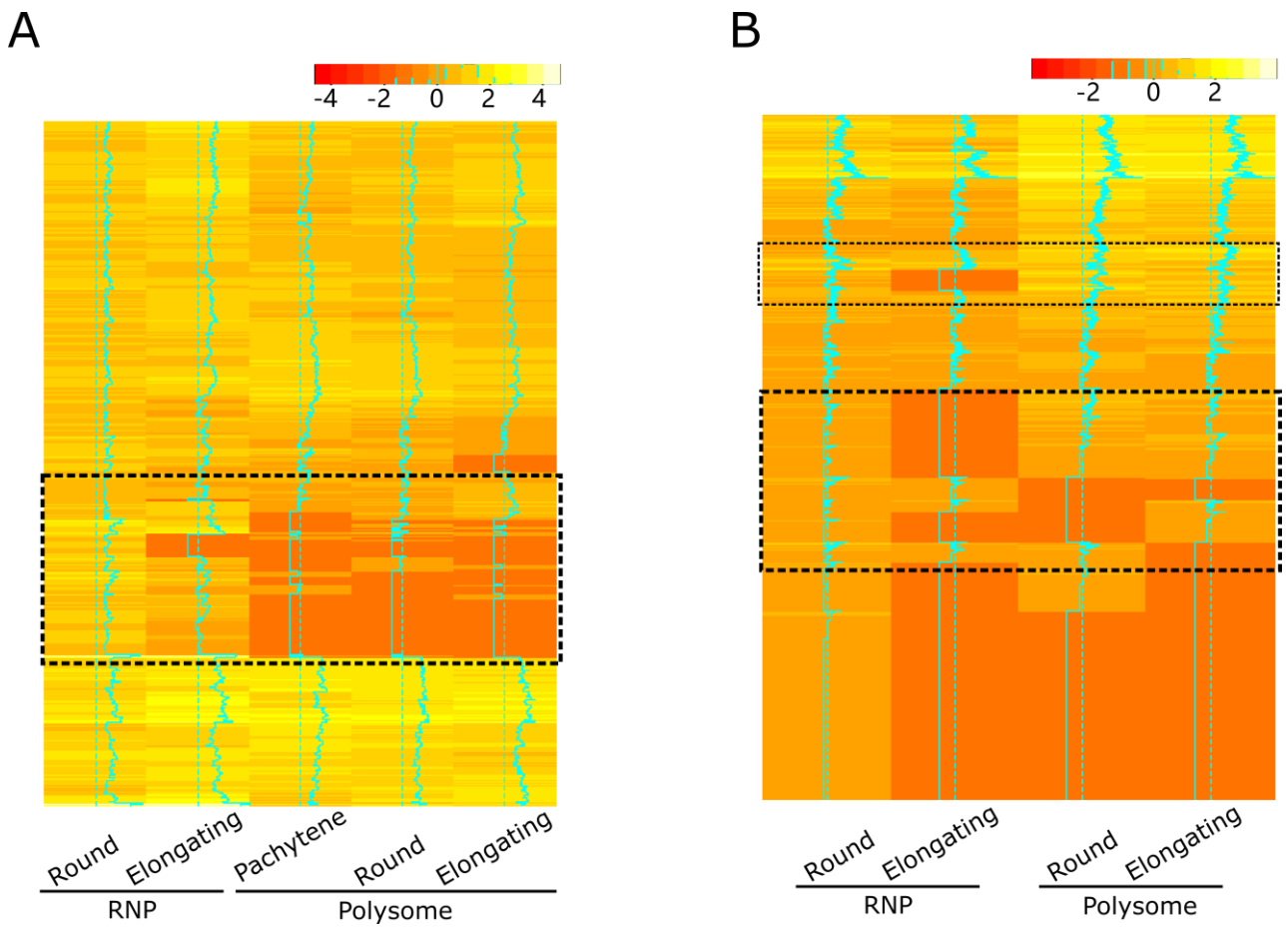

Fig. S11. Dynamic expression patterns of transcripts with shorter or longer poly(A) tails in RNP and polysome fractions in three spermatogenic cell types during spermatogenesis. (A) Heatmap showing the dynamic expression patterns of transcripts with shorter poly(A) tails (<5nt) in RNP granules of round and elongating spermatids. The transcripts with shorter poly(A) tails were stably expressed in the RNP granules from the round cell stage to elongating cell. (B) Heatmap showing the dynamic expression patterns of transcripts with longer poly(A) tails (>50nt) in the RNP granules of spermatids. The transcripts with longer poly(A) tails decrease in RNP granules, but increase in the polysome fractions. The color bar means mRNA expression level. The colors are scaled by the Z-score. Green lines running in the center of heatmaps is the value of Z-scores. Data were based on samples from two independent preparations with 3-6 mice in each, plus two technical replicates.

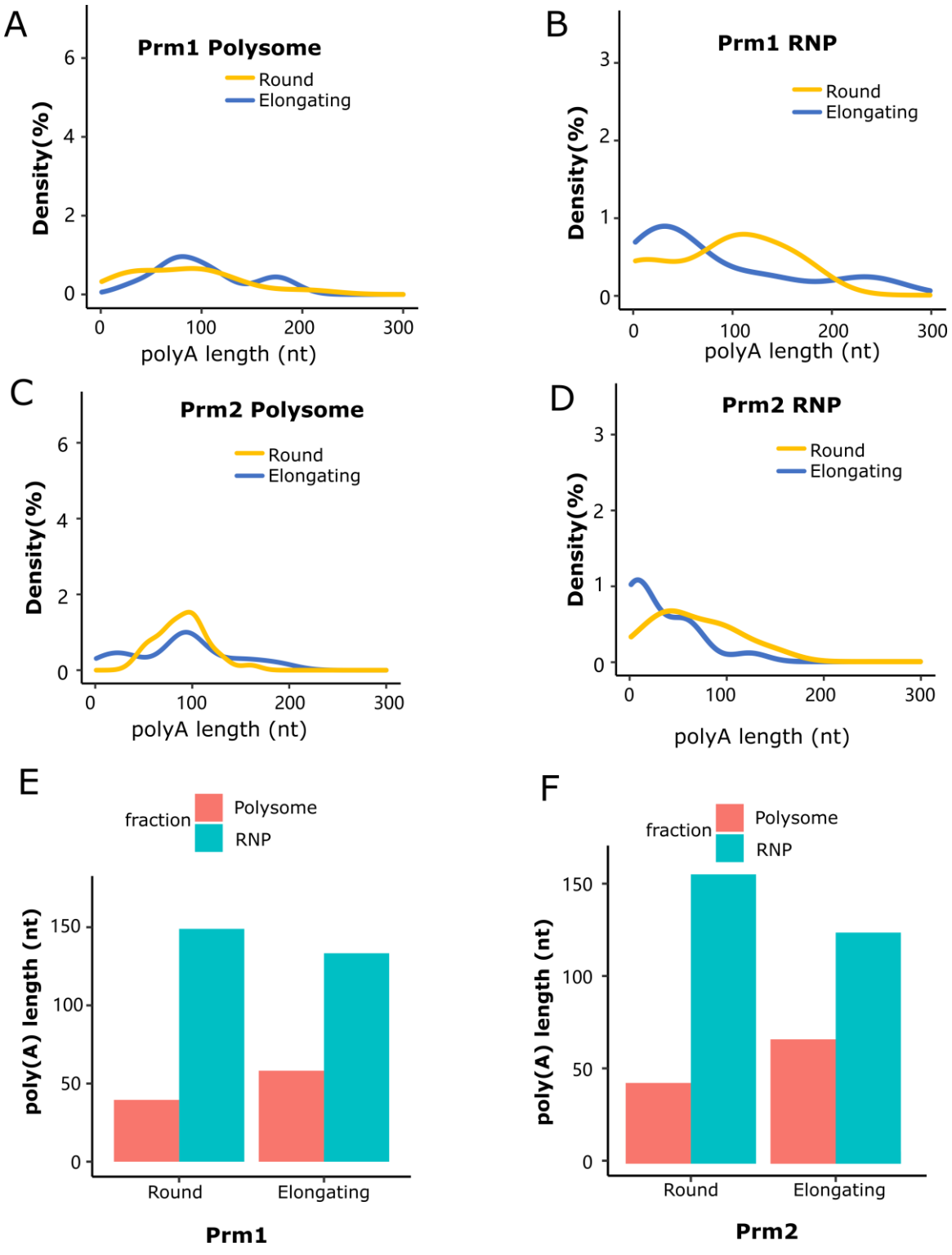

Fig. S12. The poly(A) length of protamine isoforms in spermatogenesis. (A-D) Density plots showing poly(A) length distribution of *Prm1* (A) and *Prm2* in RNP and polysome in the RNP granules of round and elongating spermatids. (E-F) The poly(A) length distribution of the most abundant Prm1/Prm2 isoform on polysome and RNP fractions.

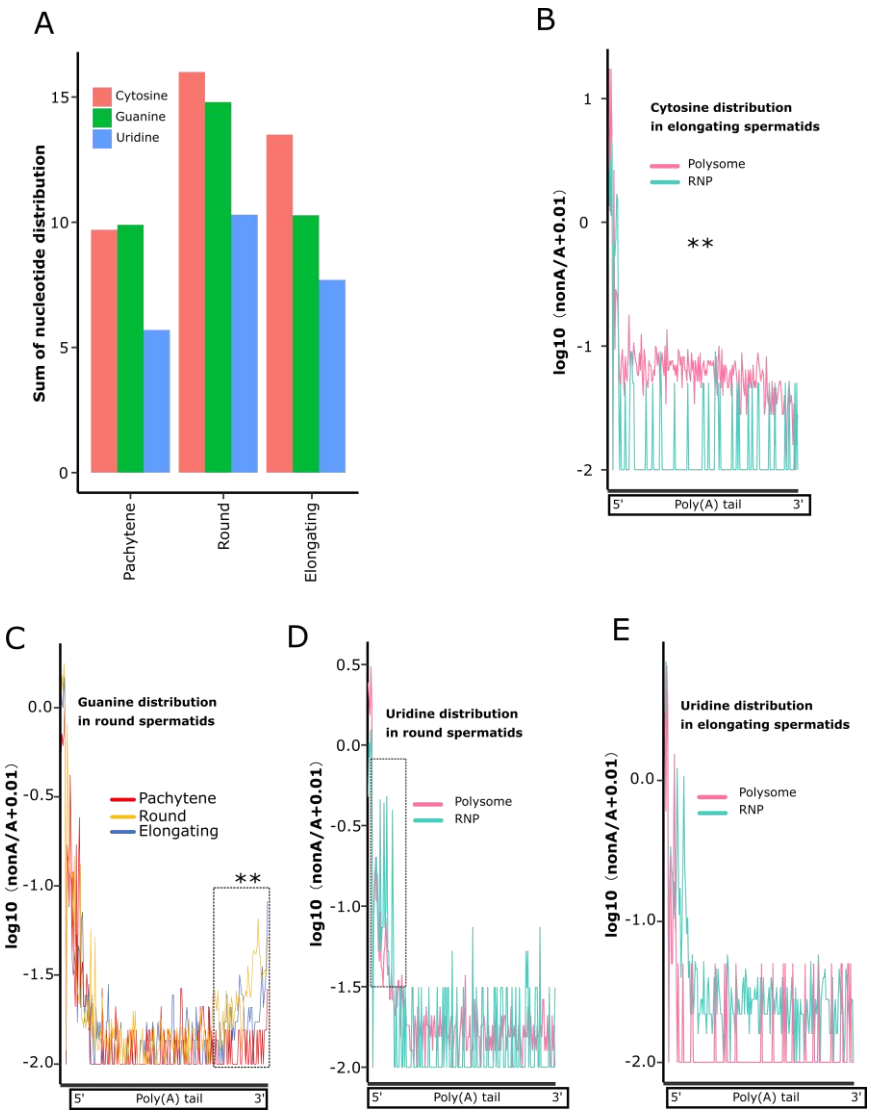

Fig. S13. Distribution of non-A nucleotides in the ploy(A) tails of transcripts during spermatogenesis. (A) Levels of non-A nucleotide contents in the poly(A) tails of transcripts in three spermatogenic cell types. (B) Distribution of cytosine in the poly(A) tails of transcripts enriched in RNP and polysome fractions in elongating spermatids. X-axis indicates the distance from each nucleotide in the poly(A) tail to the polyadenylation site. The cytosine levels in poly(A) tails are much higher (~2 folds) in RNP than in polysome fractions. **: $p < 0.05$, log t-test, number of transcripts > 10,000. Wild-type samples were from two independent preparations with 3-6 mice in each, plus two technical replicates. (C) Distribution of guanine in the poly(A) tails of transcripts in three spermatogenic cell types. X-axis means from the start of poly(A) tail to the end. **: $p < 0.05$, log t-test, number of transcripts > 10,000. Wild-type samples were from two independent preparations with 3-6 mice in each, plus two technical replicates. (D) Distribution of uridine in the poly(A) tails transcripts in RNP and polysome fractions in round spermatids. X-axis means from the start of poly(A) tail to the end. (E) Distribution of uridine in the poly(A) tails of transcripts enriched in RNP and polysome fractions in elongating spermatids. X-axis indicates the distance from each nucleotide in the poly(A) tail to the polyadenylation site. Wild-type samples were from two independent preparations with 3-6 mice in each, plus two technical replicates.

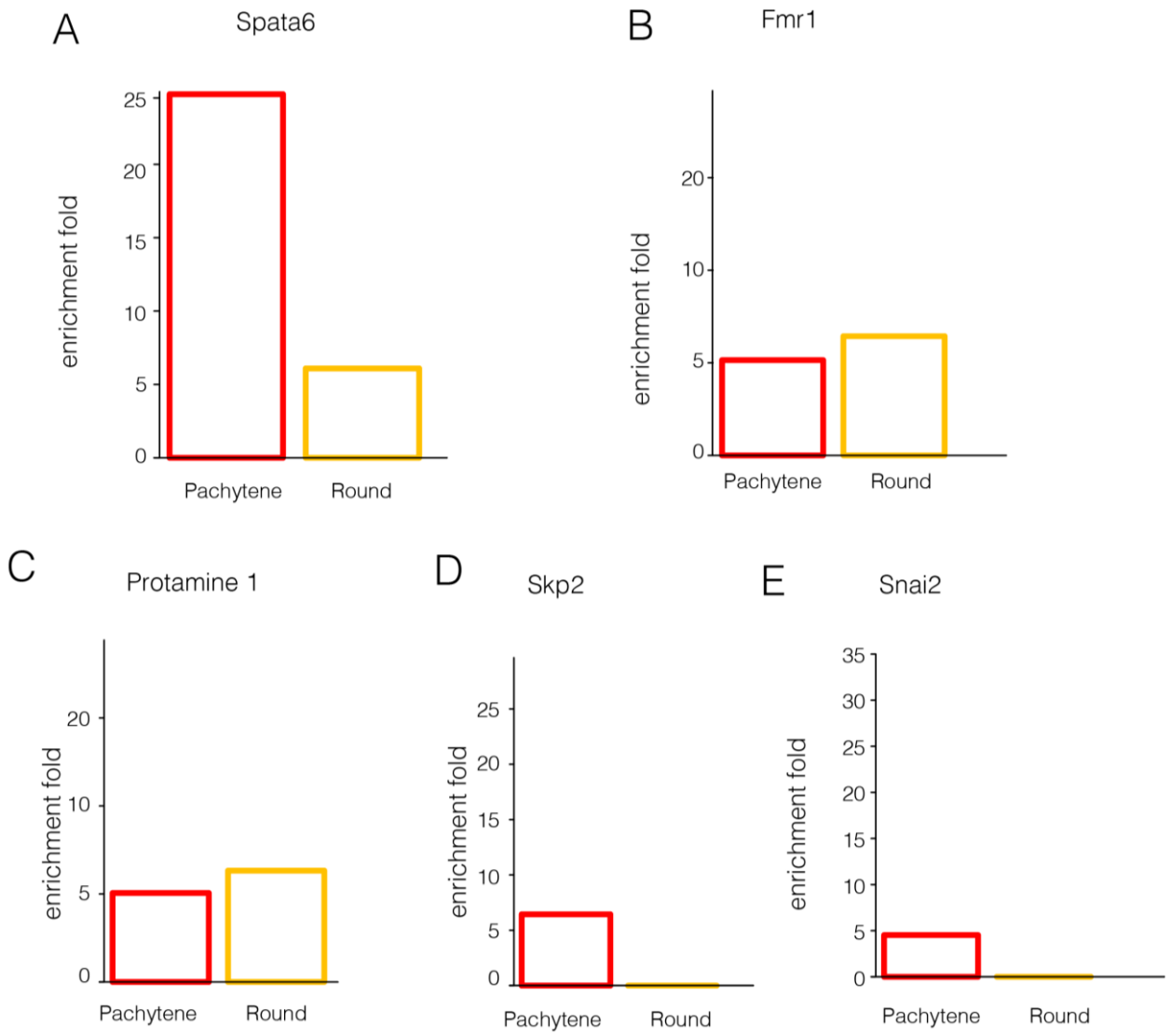

Fig. S14. The ATAC-seq analyses of the RNP/polysome-enriched genes in pachytene and round spermatocytes. Y-axis indicated the peak enrichment fold, representing the chromatin accessibility. The chromatin accessibility of *Spata6* promoter in pachytene spermatocytes were 5-fold higher than in the round spermatids. For *Fmr1, Prm1, Skp2* and *Snai2*, the chromatin accessibilities were close to background, indicating the silence of the transcription in the early stages.

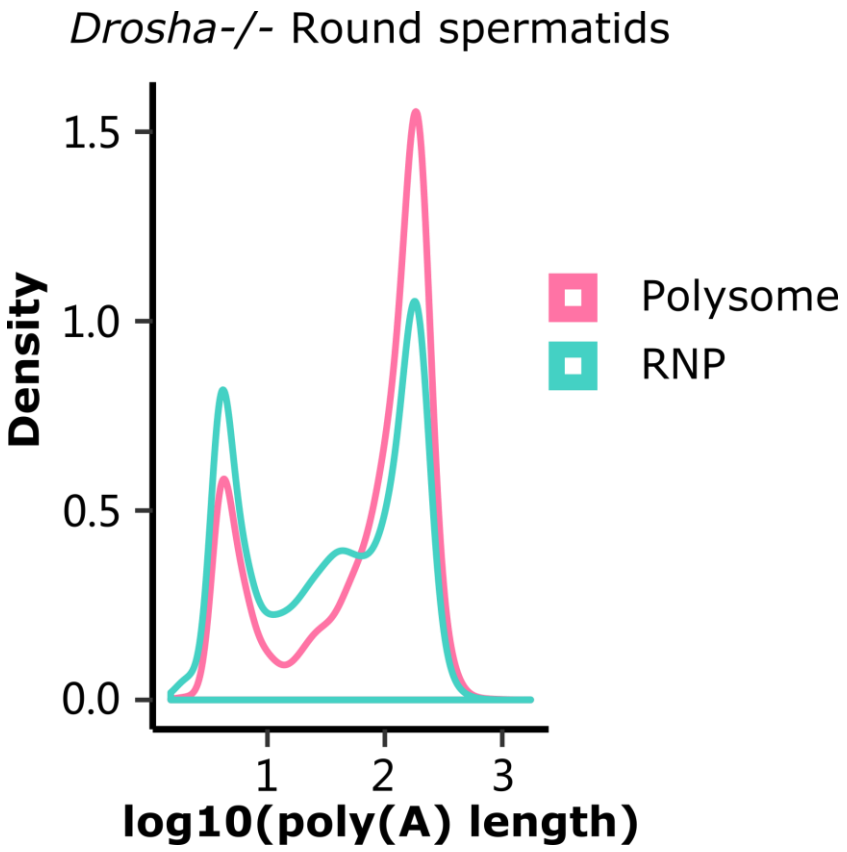

Fig. S15. The density plot showing the poly(A) length distribution in RNP granules and polysome fractions of *Drosha*-null round spermatids. The poly(A) length distribution is similar between RNP granules and polysome fractions, indicating the lack of deadenylation activity in RNP granules. Data were based on samples from two independent preparations with 3-6 mice in each, plus two technical replicates.

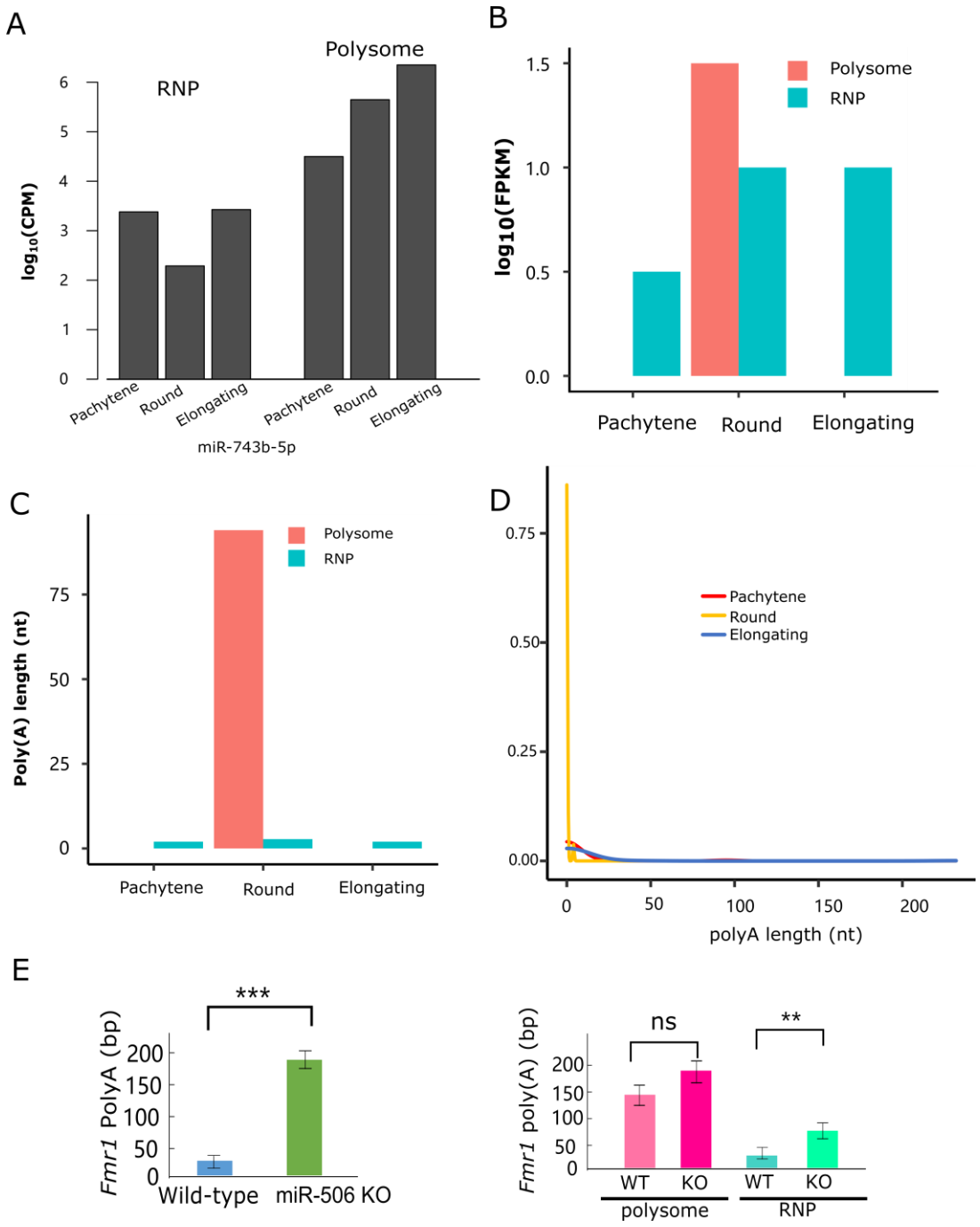

Fig. S16. The expression level of *Fmr1* and miRNA-506 family in spermatogenic cells. (A) miR-743b-5p (a member of the miR-504 family) is expressed in both RNP and polysome fractions of spermatogenic cells. (B) The majority of *Fmr1* RNAs were distributed in RNP fractions. (C) The poly(A) length of *Fmr1* showed that *Fmr1* in polysomes have longer poly(A) than in RNP fractions. (D) Density plots showing poly(A) length distribution of *Fmr1* in pachytene spermatocytes, round and elongating spermatids. (E) Histograms (left panels) calculated from Figure 4C display quantitative analyses of the data (mean ± SEM) from biological triplicates (n=3). The poly(A) tail length is quantified by our house program based on the accumulated length. Histograms (right panels) calculated from Figure 4C display quantitative analyses of the data (mean ± SEM) from biological triplicates (n=3).

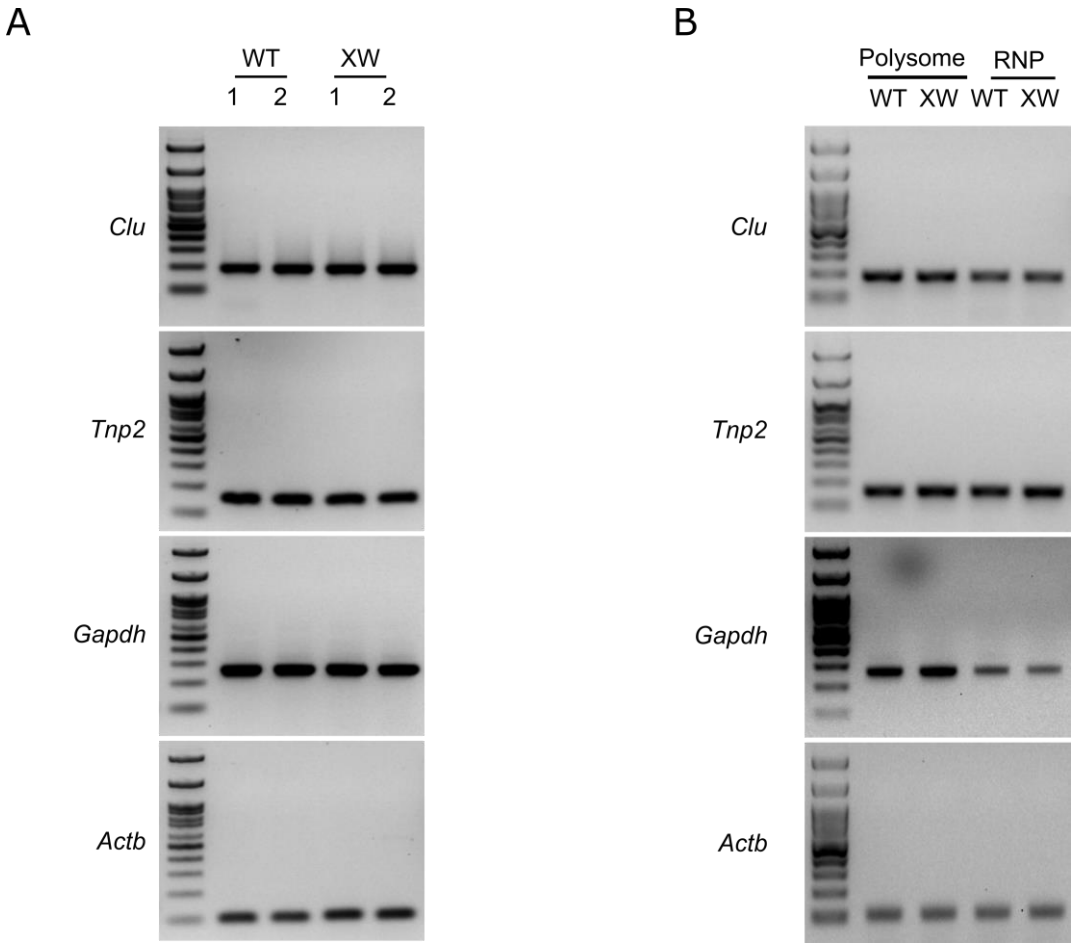

Fig. S17. Semi-qPCR validation of control genes. (A) Expression levels of four control genes (*Clu, Tnp2, Gapdh, Actb*) in the wild-type and the *miR-506* family KO (XW) testes (B) Expression levels of four control genes (*Clu, Tnp2, Gapdh, Actb*) in polysome and RNP fractions of the wild-type and miR-506 KO (XW) testes.

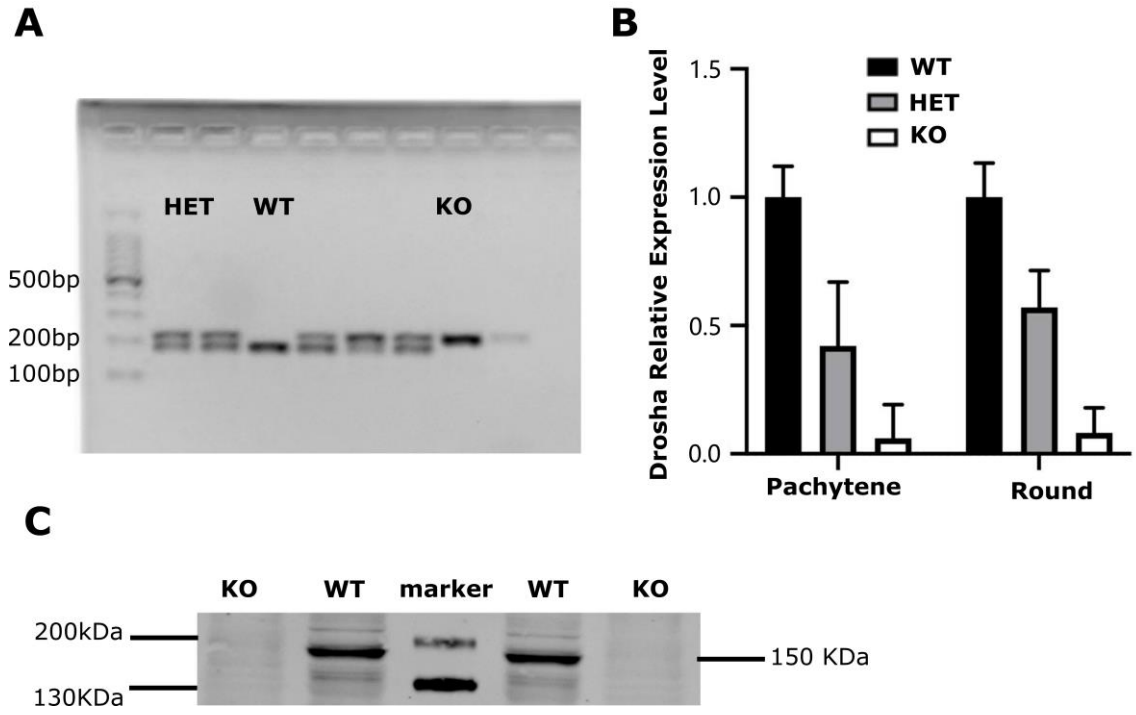

Fig. S18. (A) The genotyping results of *Drosha* cKO mice. The wild type (WT) band is 198bp and the flox band is 229bp. (B) The qRT-PCR results of *Drosha* expression in WT, heterozygous (HET) and conditional knockout (cKO) spermatogenic cells. (C) The Western bolts of DROSHA expression in WT and knockout (KO) round spermatids.

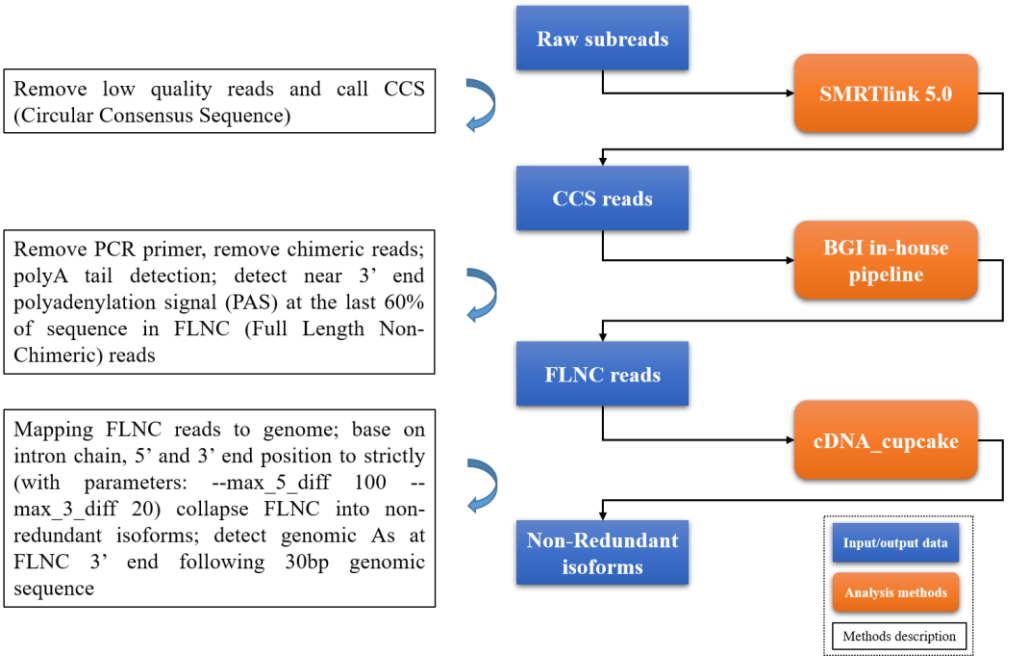

Fig. S19. The pipeline used for bioinformatic annotation of the PAPA-Seq data.

Table S1. The information of top 10 isoforms of *Prm1*, *Prm2* and *Spata6*

GeneID	Isoform ID	Isoform Length (bp)	Read Counts	3'UTR start position	PAS start position	PAS motif
Prm1	PB.127204.429(19118)	553	32295	380	536	AATAAA
Prm1	PB.127159.35(19118)	368	19	NA	351	AATAAA
Prm1	PB.127204.449(19118)	368	12	NA	351	AATAAA
Prm1	PB.127204.503(19118)	378	11	NA	373	AATAAA
Prm1	PB.127204.507(19118)	383	8	NA	378	AATAAA
Prm1	PB.127204.428(19118)	322	5	NA	305	AATAAA
Prm1	PB.127204.469(19118)	373	5	NA	368	AATAAA
Prm1	PB.127204.440(19118)	341	5	NA	324	AATAAA
Prm1	PB.127204.464(19118)	386	2	NA	381	AATAAA
Prm1	PB.127159.36(19118)	368	2	NA	351	AATAAA
Prm2	PB.127204.311(19119)	513	4	429	503	AATAAA
Prm2	PB.127204.362(19119)	533	3	NA	523	AATAAA
Prm2	PB.127159.28(19119)	1028	3	964	NA	NA
Prm2	PB.127204.375(19119)	599	3	498	589	AATAAA
Prm2	PB.127204.303(19119)	603	2	502	593	AATAAA
Spata6	PB.234919.860(67946)	1136	906	714	1123	AATGAA
Spata6	PB.234919.665(67946)	2450	433	451	2384	AATGAA
Spata6	PB.234919.380(67946)	2425	414	1651	2353	AATGAA
Spata6	PB.234919.713(67946)	2505	46	707	2460	AATGAA
Spata6	PB.234919.807(67946)	2309	46	1249	2264	AATGAA
Spata6	PB.234919.846(67946)	1427	13	1099	1187	TTTAAA
Spata6	PB.234919.668(67946)	1985	11	1406	1882	ACTAAA
Spata6	PB.234919.843(67946)	1128	7	1067	1115	AATGAA
Spata6	PB.234919.840(67946)	988	6	927	975	AATGAA
Spata6	PB.234919.842(67946)	1171	6	1067	1155	TTTAAA

PAS: Alternative Polyadenylation Site. The UTR is predicted by transdecoder. The PAS is predicted by BGI in-house pipeline.

Table S2. Primers used in this study

Name	Sequences	Usage
miR465 Ext F	GGCCTGATCTATTCTGAAGGGA	Genotyping
miR465 Ext R	ATCTCACAAATGCCTTTCCGA	Genotyping
miR465 Int R	GATGAGCTTGCACATATCCACA	Genotyping
RT primer 1	GGTAATACGACTCACTATAGCGAGA NNNNNNNNNNCCCCCCCCCTTT	Reverse transcription
Fmr1 3'UTR F2	GCCGTTATTTACCAACTTTCAAGAACGT	PCR
PCR primer 1	GGTAATACGACTCACTATAGCGAG	PCR
Fmr1 qPCR F	AAAAGTCCAGAGGGTGTTAGTGGTTTCATC	PCR & qPCR
Fmr1 qPCR R	TTCAGGTGATAATCCAAAAGAACAGTGGCA	PCR & qPCR
Skp2 3'UTR F	GTATTTCCGTGCTACAATCCATTTCTAT	PCR
Snai2 3'UTR F	CAACTGAATGAACTCTGTATGAAAGTGA	PCR
Actb F	CGCCACCAGTTCGCCATGGA	PCR & qPCR
Actb R	TACAGCCCGGGGAGCATCGT	PCR & qPCR
Gapdh F	ACAGTCCATGCCATCACTGCC	PCR & qPCR
Gapdh R	GCCTGCTTCACCACCTTCTTG	PCR & qPCR
Clu F	GTGTCACTGAGGTGGTGGTG	PCR & qPCR
Clu R	ATTCCCTCCCAGACACTCCT	PCR & qPCR
Tnp2 F	TCGACACTCACCTGCAAGAC	PCR & qPCR
Tnp2 R	CCTGGAGTGCGTCACTTGTA	PCR & qPCR
Prm1-F	CAGCAAAAGCAGGAGCAGAT	PCR
Prm1-R	CGAGATGCTCTTGAAGTCTGGT	PCR
Prm2-F	AAATGTAGGAGGCACCATCACT	PCR
Prm2-R	TCTCGTGTCAAGCTTTATTTGG	PCR
Tnp1-F	GAGAGGTGGAAGCAAGAGAAAA	PCR
Tnp1-R	CCCACTCTGATAGGATCTTTGG	PCR